European Journal of Mechanics / B Fluids 108 (2024) 1–31

Contents lists available at ScienceDirect

European Journal of Mechanics / B Fluids

journal homepage: www.elsevier.com/locate/ejmflu

On the design of manifolds for parallel channel systems

Yaser Hadad [*,1], Ghazal Mohsenian [1], Paul Chiarot, Bahgat Sammakia

Department of Mechanical Engineering State University of New York at Binghamton, Binghamton, NY, USA

ARTICLE INFO

Keywords:
Flow Distribution
Pressure Drop
Eddies
Parallel Channels
Complementary Designs
Wall Friction Effect
Uniformity

ABSTRACT

In the design of high-performance heat and mass transfer devices such as liquid-cooled heat sinks, catalytic reactors, and catalytic convertors, parallel mini/microchannels are favored owing to their special potentials. Offering low pressure drop, providing high transfer surface area to volume ratio, and being easy to manufacture and optimize have been drawing thermal and chemical engineers attention to parallel channels for past decades. When working with parallel channels, the challenge of flow maldistribution is commonly faced which decreases their efficiency significantly. System total pressure drop and flow uniformity are two parameters that determine the system performance. In the present study, a variety of practical ideas, aiming to enhance parallel channels performance, are studied numerically. Inventive manifold designs with high hydraulic performance are created through the course of this study. The results of these designs are compared with basic conventional designs which show substantial enhancement. Analyzing less successful designs lead us to deep understanding of fluid dynamics in parallel channel heat and mass transfer devices.

1. Introduction

In the field of engineering, the word “manifold” is an umbrella term covers certain types of fluid dynamics components which distribute a flow to a set of mechanisms typically working based on transport phenomena. In most application, manifolds also collect the flow from those mechanisms at the end of the process (energy and/or mass transfer) and direct it to an exit. Despite the same functionality, manifolds could be in a wide range of size and diverse geometries depending on their application. Manifolds are designed and used for various applications including but not limited to liquid-cooled heat sinks, chemical processing systems, catalytic microchannel reactors, catalytic converters, fuel cells, heat exchangers, data centers racks and air conditioning, internal combustion engines, solar receivers, and irrigation. As the efficiency of these systems is intensely affected by manifold performance, providing practical optimal manifold designs that fit them is crucial and creative. Fig. 1 demonstrates three manifolds designed for different applications. Fig. 1(a) shows a manifold used in space industry (shuttles), Fig. 1(b) and (c) illustrate manifolds used in electronic packaging (liquid cooled heat sinks), and agricultural (irrigation) industries.

In primary studies [1–5] researcher’s approach was to apply the integral form of continuity, momentum, and energy equations to one-dimensional conduits with lateral branches of inflow and outflow. Using this approach, they developed closed-form solutions which can predict flow and pressure distribution to some extent. From their analytical models, dimensionless parameters characterizing the performance of manifolds were formulated. One of the important application of manifolds occurs in internal combustion engines used in different power-generating devices. Low pressure drop intake manifolds are critical to maximize the mass of the drawn air into the cylinders. Moreover, the intake manifolds ensure that the air is sent to the cylinders in equal mass to make piston movements stable and compatible and resulting in engine maximum efficiency. Using computational fluid dynamics (CFD) Gocmen and Soyhan [6] solved and optimized their new design for internal combustion engines. They showed that their design outperforms conventional designs because it is symmetric and, distributes the mainstream in two steps before entering the cylinders. When designing intake manifolds, it is crucial to make their geometry adaptable to changes in flow behavior to ensure maximum performance throughout the engine speed range. Talati et al. [7] developed a one-dimensional model of the Stock engine to design and optimize a multi-throttle variable-length intake manifold on a four-stroke four--cylinder engine. In addition to the variable length system, their design uses a different combination of open throttle bodies to adapt its performance with engine speed and provide high volumetric efficiency. By using a numerical one-dimensional model conducted on an Otto engine,

* Corresponding author.
E-mail address: yhadad1@binghamton.edu (Y. Hadad).
[1] Both the first author, Dr.Hadad, and the second author, Dr.Mohsenian, contributed equally to this paper.

https://doi.org/10.1016/j.euromechflu.2024.07.004
Received 2 April 2024; Received in revised form 9 June 2024; Accepted 1 July 2024
Available online 6 July 2024

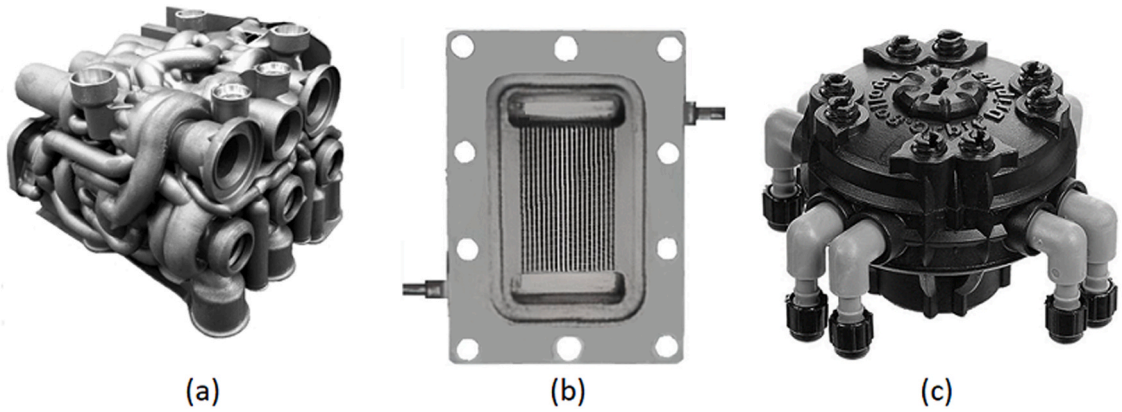

Fig. 1. Manifolds with different geometries for various applications (a) space industry, (b) electronics cooling, and (c) irrigation.

Souza et al. [8] investigate the effect of different intake manifolds geometries on the engine efficiency. They composed an experimental apparatus to measure the volumetric efficacy of the engine for different designs of the intake manifolds. They improved the engine volumetric efficiency by 6 % at 3500 rpm by proposing a new design. In the technology of fuel cells, uniform distribution of reactants supplied to each individual cell is of great importance because the performance of a stack is limited by the single cell which receives the minimum flow. Manifolds with different geometries such as serpentine, U-, I-, and Z-type have been designed to improve the flow distribution uniformity in fuel cells thorough Maharudrayya et al. [9]. Using one dimensional continuity and momentum equations, Kee et al. [10] develop a computational model to predict pressure drop and flow distribution in the small channel network which are typical in planar fuel cells. The solutions were presented in graphical form with non-dimensional groups to generalize the results without the need to solve the model for other applications. The channel network of fuel cell systems is like header channel configuration of plate and frame heat exchangers and hence the results can be used for similar applications. Using the analogy between fluid flow and electrical network, Zhang et al. [11] presented an analytical model in the form of matrix equations, to estimate the flow distribution in ladder (parallel channel) configurations for proton exchange membrane fuel cells. After validating the model with three-dimensional CFD simulations, it was used to optimize Z-type and U-type configurations. Using CFD, Dong et al. [12] designed and optimized a tree-type modular manifold for flow uniformity and overall pressure drop. They calculated channels' equivalent diameter based on the principle of minimizing entropy generation. Chen et al. [13] characterized a U-type manifold used for a two-dimensional stack composed of seventy-two cells. They investigated pressure variation and flow distribution for channels with different flow resistances, manifold widths, and flow rates. A discrete approach is developed by Wang and Wang [14] to find a design that meets the requirements of flow uniform distribution and pressure drop in single serpentine, multi-serpentine, and parallel channel configuration used in fuel cells. Flow distribution with Z-type arrangement was formulated by applying mass and momentum equations to distributing and collecting manifolds. Maharudrayya et al. [15] developed one-dimensional analytical models based on mass and momentum balance equations for parallel channels of Z- and U-type configurations. They obtained closed-form solutions for the flow distribution in individual channels and for the pressure drop over the entire distribution plate. They validated their models by comparison with results calculated by three-dimensional CFD simulations. In a complimentary study, they extended their analytical solutions obtained for single U- and Z-type flow configurations to multiple U- and multiple Z-type flow configurations of interest to fuel cell applications [9]. Wang [16,17] developed theoretical models based on mass and momentum conservation to solve pressure and flow distribution of U- and Z-type fuel cell configurations. Using his explicit analytical solution, he performed a parametric analysis through five general characteristic parameters representing geometrical structures and flow conditions of the fuel cells. In another study Wang [18] generalized his theoretical models to cover both continuum and discrete manifolds with arbitrary geometry. Catalytic microchannel reactors are heat and mass transfer systems which are very similar to parallel channel cold plates both in geometry and function. By taking the advantage of mini and microchannels, mini/-microchannel reactors enable chemical reactions to occur at rates 10–1000 times faster than in conventional systems. Microreactors offer other advantages over conventional scale reactors such as safety, reliability, scalability, and finer degree of process control. Like fuel cells, the performance of microreactors is affected severely by channel flow distribution. Commenge et al. [19] developed an approximate pressure drop model to predict and optimize the uniformity of flow through channels. They validated their approximate model by a detailed finite-volume calculation. Catalytic converters are exhaust emission control devices used with internal combustion engines to convert toxic gases and pollutants in exhaust gas in to less-toxic pollutants by catalyzing a redox reaction. Catalytic converters are mass and heat transfer devices whose performance depends on flow distribution. Nonuniform flow distribution causes significant radial temperature and concentration gradients that can severely degrade the performance of converter. Zygourakis [20] studied the effect of flow distribution on the performance of catalytic converters. Heat exchangers are a macroscale example of heat transfer devices receive the benefit of manifolds for uniform flow distribution. The maldistribution of flow deteriorates thermal and hydraulic performance of heat exchangers and induces local heterogeneity in temperature and pressure fields. Thonon et al. [21] developed a numerical model to predict flow distribution in plate heat exchangers. They found that thermal efficiency is less affected by a nonuniform flow distribution than the overall pressure drop. However, they observed a significant temperature heterogeneity at the outlet of the channels resulted from flow maldistribution. Rao et al. [22] conducted experimental studies to investigate the influence of flow nonuniformity on the pressure drop and thermal performance of plate heat exchangers. Considering U-type and Z-type plate heat exchanger, they distinguished major parameters (port size, number of channels, flow rate, etc.) and estimated their effectiveness. Based on an analytical solution of continuity and momentum equations, Bassiouny and Martin [23] introduced a general characteristic parameter (m^2) for U- and N-type manifolds used in plate heat exchangers which determines the flow behavior. Their characteristic parameter (m^2), expressed in terms of cross-sectional area of the intake and exhaust conduits and channels, flow velocity in the intake and exhaust conduits, axial components (normal to channels flow) of flow velocity at channels' inlet and outlet, and average total head loss coefficient for channel flow. They found that channel flow rate increases and decreases in the direction of the intake

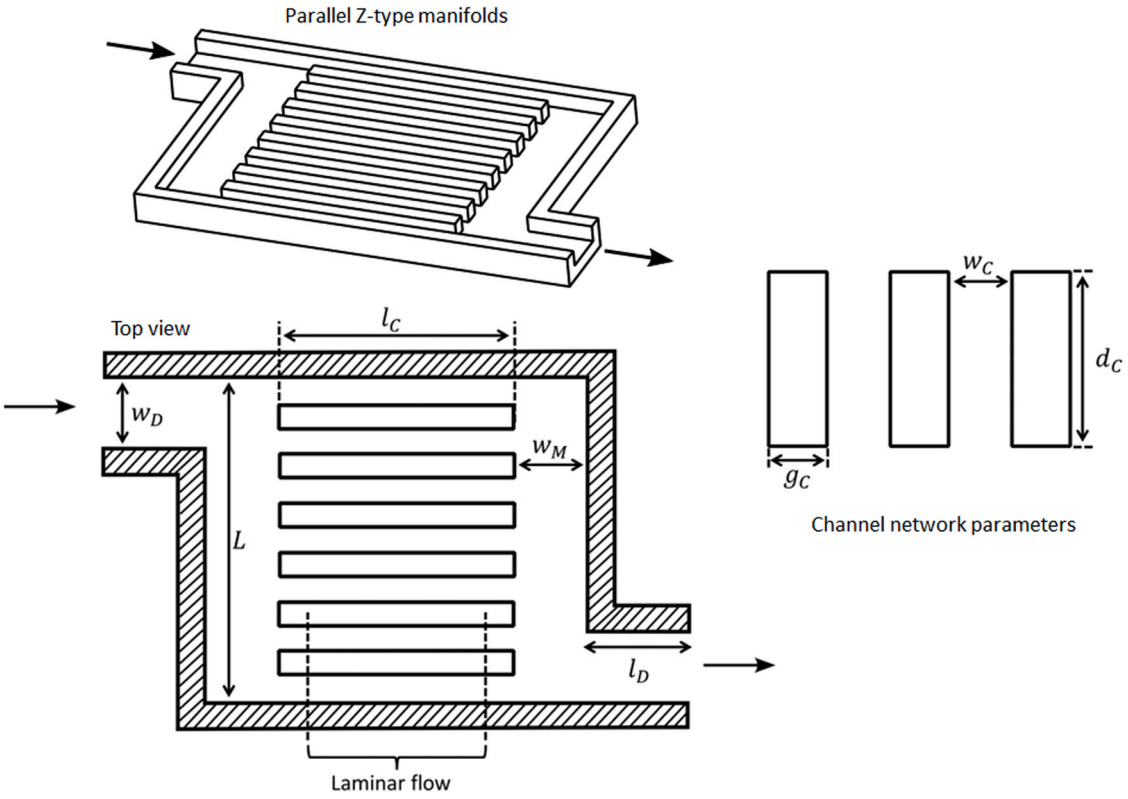

Fig. 2. Geometric parameters of the channel network-manifold system.

stream when m^2 is negative and positive, respectively. The flow distribution tends to be uniform for low values of m^2 ($0 < m^2 < 0.01$) and is perfectly uniform when m^2 is zero. Beckedorff et al. [24] measured pressure drop, flow distribution, and heat transfer rate in a commercial shell and plate heat exchanger. They estimated the effect of flow maldistribution on the shell and plate sides. Parallel-tube solar receivers are heat transfer devices which benefit N-and U-type manifold to a high extent. Hao et al. [25] evaluated the hydrodynamic characteristics of evaporation panels in a solar receiver. The effect of heat flux concentration ratio, total flow rate, and system pressure on the flow distribution of parallel tubes was studied. Liu et al. [26] analyzed steam-water two-phase distribution in parallel heated pipes by numerical modeling. They verified and used their model to investigate the effects of system pressure, inlet steam quality, and manifold type on the flow distribution. Uhlig et al. [27] used tabular headers assembled in ring-shape to distribute and collect flow through their solar tower receiver. Design and performance analysis of manifolds used in mini/micro-channel systems such as liquid-cooled heat sinks, usually known as cold plates in industry, fuel cells, and microchannel catalytic reactor are the focuses of this study. An analytical model based on one-dimensional flow network was developed by Saeed and Kim [28] to modify inefficient shapes of distributor and collector in conventional liquid cooled parallel microchannel heat sinks. Although their proposed design was challenging to manufacture, it provided significant improvement in pressure drop and flow uniformity. Bogojevic et al. [29] used a flow resistance network model to study the effect of various parameters such as distribution and collection manifolds geometry, and positions of inlet and outlet holes. They compared the result of their approximate model with three-dimensional CFD. Additionally, effect of flow blockage on flow distribution and pressure drop was investigated. Cho et al. [30] developed a one-dimensional analytical model for a two-phase microchannel heat sink used for cooling integrated circuits with nonuniform power map. The model was used for minimizing flow nonuniformity and heat sink pressure drop. A three dimensional based optimization method was developed by Tonomura et al. [31] to determine optimal manifold shape for plate-fin microdevices under the constraint of flow uniformity. A two-dimensional resistive model was developed by Tondeur et al. [32] to find designs providing uniform flow distribution among rectangular lattice network and parallel channels with different compactness. They analyzed different Z-type and U-type circuits under the constraint of optimal uniform. Location and direction of flow inlet and outlet can remarkably affect both pressure drop and thermal performance of liquid cooled heat sinks. Five basic designs with different inlet-outlet arrangement and flow direction (parallel and vertical to channels) were analyzed for flow distribution in parallel channel cold plates by Lu and Wang [33] using CFD. A detailed three-dimensional numerical simulation was used to identify the optimal geometric parameters that provide enhanced heat transfer and flow distribution in microchannel heat sink by Xia et al. [34]. In their parametric study, they examined the effect of manifolds shape (triangular, trapezoidal, and rectangular), perpendicular inlet and outlet ducts' locations (I-, U-, and Z-type), and channels cross-sectional shapes (conventional rectangular microchannels, and microchannels with offset fan-shaped and triangular reentrant cavities). Using the strategy of pin-fin arrays in the inlet manifold of parallel mini-channel heat sinks, Song et al. [35] aimed to increase flow uniformity without a pressure drop penalty. The combination of two different manifold shapes, trapezoidal and rectangular, with ten different pin-fin arrangement were solved numerically to investigate flow uniformity within channels. In an experimental-numerical study, Manikanda Kumaran et al. [36] estimated the effect of manifolds geometry and inlet-outlet configuration on flow distribution in microchannel heat sinks. They validated their numerical simulation by experimental results and used it for performance analysis and finding the roots of flow maldistribution in different designs (parallel and perpendicular U-, Z-, and I-type manifolds). A detailed experimental investigation with the focus on manifold shape (rectangular, triangular, and trapezoidal) and inlet configuration (inline and vertical) was carried by Anbumeenakshi and Thansekhar [37] to

Table 1
Geometric and operational fixed parameters.

Symbol	Definition	Value
l_C	Channel length	$45mm$
l_D	Inlet and outlet ducts' length	$10mm$
L	Channel network width	$57mm$
w_D	Inlet and outlet ducts width	$9mm$
w_M	Inlet and outlet manifolds width	$10mm$
d_C	Channel depth (fin height)	$3mm$
g_C	Channel gap (fin thickness)	$1mm$
w_C	Channel width (fin gap)	$1mm$
N	Number of channels	28
Q_E	Total flow rate of the system	$25cm^3/s$ $(1.5LPM)$
μ	Dynamic (absolute) viscosity of the fluid	$0.000855\ kg/m.s$
ρ	Density of the fluid	$997\ kg/m^3$

minimize flow maldistribution in parallel channel heat sinks. Cho et al. [38] experimentally investigated cooling performance and pressure drop of parallel microchannel heat sinks under uniform and nonuniform heat flux conditions for different geometries of channels and manifolds. They fabricated and tested four microchannel heat sink designs achieved by combining straight or diverging channels with rectangular or trapezoidal manifolds. By solving the two-dimensional equations of motion (continuity and Navier-Stokes) numerically for a generic manifold system for parallel channels, Tong et al. [39] identified eight geometry-based strategies for attainment of uniform flow distribution. Governing equations for three dimensional conjugate (conduction-convection) heat transfer were solved numerically by Chein and Chen [40] to investigate the effect of inlet/outlet arrangement on thermal and hydraulic performance of microchannel heat sinks.

According to literature review, many researchers have investigated fluid flow through parallel channels equipped with basic conventional manifold designs (U-, Z-, N-, and I-type). Their aims have mainly been providing compact models, accurate enough, to predict pressure drop and flow distribution as well as system performance improvement. To do so, they studied the effect of distributor and collector shape and dimension, inlet/outlet location, and shape of microchannel. The aim of this study however is to bridge the gap between commercial widely used designs and today's industry need. Detailed three-dimensional numerical simulations are used to study classic designs and then estimate the performance of introduced novel designs obtained by their combination.

2. Problem description

In this study, the performance of manifolds with different designs is estimated by linking up them with a fixed parallel channel system. The performance is translated to whole system (inlet and outlet ducts, channel network, and manifolds) pressure drop and flow distribution uniformity. System pressure drop is calculated by subtracting the pressure at the exit of the outlet duct (P_{out}) from the pressure at the entrance of the inlet duct (P_{in}).

$$\Delta P = P_{in} - P_{out} \tag{1}$$

The lower ΔP system offers, the lower pump work is required and there is lower possibility of leaking at the inlet and outlet connectors.

The standard deviation of flow distribution among the channels is considered as a measure of flow uniformity. The standard deviation is defined as follows.

$$S.D = \sqrt{\frac{1}{N}\sum_{i=1}^{N}(Q_{iC} - \overline{Q}_C)^2} \tag{2}$$

where N is the number of channels, Q_{iC} is i^{th} channel flow rate, and $\overline{Q}_C$ is channels average flow rate.

$$\overline{Q}_C = \frac{\sum_{i=1}^{N} Q_{iC}}{N} \tag{3}$$

The lower the standard deviation, the more uniform flow distribution is formed throughout the channel network. The standard deviation of zero is obtained where the flow is distributed perfectly uniform in channels. To have a fair comparison, the geometry of the channel network, the space available for inlet manifold (distributor) and outlet manifold (collector), flow rate, and fluid properties are fixed for all manifold designs. Fig. 2 depicts the geometric parameters of the channel network-manifold systems that are assumed to be fixed in this study. Although a parallel Z-type manifold (baseline) is used to show fixed geometric parameters, these parameters have the same value for all other manifold designs. The values of fixed geometric parameters associated with fixed operational parameters (fluid flow rate, and thermo-physical properties) are stated in Table 1. Themo-physical properties of water at $300K$ is used for all designs.

3. Numerical solution

3.1. Basic assumptions

The flow regime in inlet and outlet ducts is considered turbulent due to the high flow Reynolds number there.

$$\mathrm{Re}_D = \frac{\rho V_D D_{D,h}}{\mu} = \frac{2\rho Q_E}{\mu(w_D + d_C)} \tag{4}$$

In Eq. (4) V_D and $D_{D,h}$ are duct flow velocity and hydraulic diameter, respectively. Inlet and outlet ducts Reynolds number is 4859, for the flow rate of 1.5 LPM, which significantly is above the transient value for internal flows (2300). Flow regime across the manifolds is assumed turbulent because it includes factors which increase rate of turbulence such as sudden expansion and contraction, sudden change in flow direction and recirculating eddies. To consider the transition from turbulent to laminar and the reverse, 10 % of the channels' length at the beginning and end is solved using turbulence model of $k-\varepsilon$.

The of rest of the channels, 80 % in the middle, is solved by laminar model as channel Reynolds number is less than 1000. Other simplifying assumptions applied to the computational solution can briefly expressed as follows:

- Flow is three dimensional, incompressible, and steady.
- The effect of gravity is negligible.
- The thermo-physical properties of the fluid are constant.
- The viscous dissipation is neglected.

3.2. Governing equations

Mass and momentum conservation equations simplified according to the basic assumptions are expressed as follows.

Conservation of mass

$$\nabla \vec{V} = 0 \tag{5}$$

Conservation of momentum

$$\rho\left(\vec{V}.\nabla\right)\vec{V} = \nabla P + \mu\nabla^2\vec{V} \tag{6}$$

where $\vec{V}$ and P are velocity and pressure fields, respectively. ρ is fluid specific mass and μ denotes fluid absolute viscosity.

A constant pressure and inlet velocity boundary conditions are applied on the exit of the outlet duct and entrance of the inlet duct, respectively. No-slip boundary condition is exerted on all solid walls.

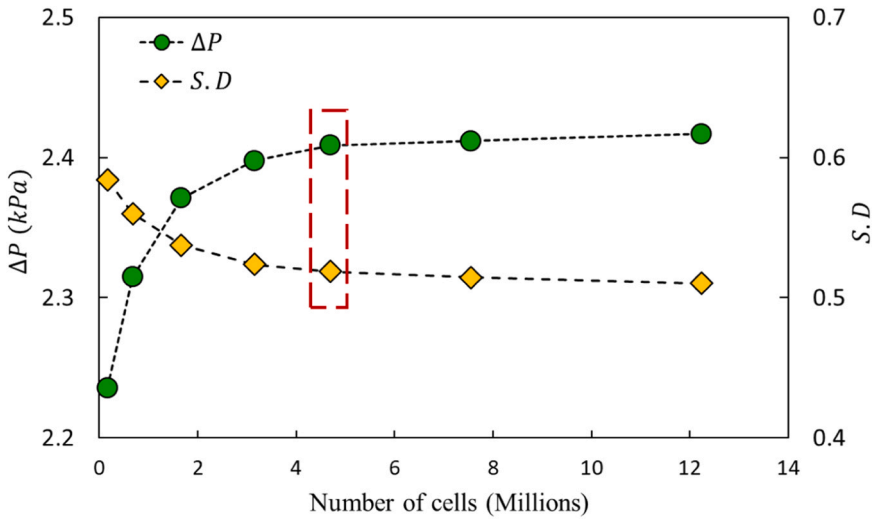

Fig. 3. The results of the discretization error analysis based on pressure drop and flow distribution standard deviation (the grid with 4.7 million cells is adopted).

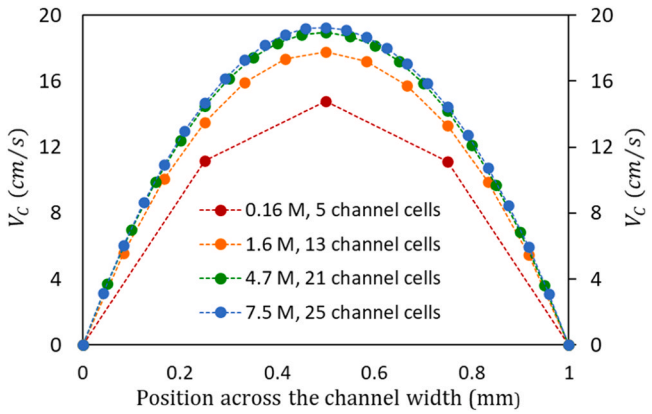

Fig. 4. Channel velocity profile for grids with different total and across-the-channel cells numbers.

3.3. Numerical analysis

Numerical analysis is performed using ANSYS Fluent which uses finite volume method to discretize the system of governing equations in the domain of solution on a staggered grid. The second order upwind and central difference schemes are used for spatial discretization of the convective and diffusion terms, respectively. The iterative SIMPLE algorithm is used to solve the governing equations and calculate the velocity and pressure fields. SIMPLE algorithm is used to address the pressure-velocity coupling of the equations of motion. Mapped structured grids with hexahedral cells is applied to the computational domains of different designs. The realizable $k-\varepsilon$ model was used to treat the turbulent transport in the inlet and outlet ducts, manifolds and 10 % of the entrance and exit of the channels. Realizable $k-\varepsilon$ turbulence model is adopted in this study as it provides superior performance for flows involving rotation, boundary layers under strong adverse pressure gradients, separation, and recirculation than other turbulent models usually used for small computational domains (standard $k-\varepsilon$, RNG $k-\varepsilon$, $k-\omega$, Spalart-Allmaras, etc.)[41,42].

3.4. Discretization error

A discretization error analysis is performed for the baseline design (Z-type manifold) based on pressure drop and flow uniformity. The results of this discretization error analysis are illustrated in Fig. 3. By increasing the number of cells from almost 4.7 to 7.5 million, the response parameters (ΔP and $S.D$) show a variation less than 1 %. Therefore, a grid with almost 4.7 million cells is selected for this design.

In addition to response parameters the channel velocity profile variation is considered with grid cell numbers. As the grid gets finer, the number of cells across, along, and in the height of channels increase proportionally. As it can be seen in Fig. 4 the channel velocity profile approaches a unique parabola by increasing the number of cells across the channel.

3.5. Model validation

To validate the modeling methodology, the numerical results of the pressure drop are compared with experimental data for an available prototype shown in Fig. 5(a). The prototype is a parallel channel water cooled heat sink (cold plate) possesses 136 fins with height, thickness, and gap (channel width) of 4.8 mm, 0.15 mm, and 0.2 mm, respectively. A Z-type manifolds distribute the coolant into the channels. The geometry of the prototype is developed accordingly and solved for pressure drop. Fig. 5(b) compares the numerical solution and experimental measurements of the prototype pressure drop at three values of water flow rate at 300 K. The numerical results are in a good agreement with experimental data. The maximum and average discrepancies are less than 7 % and 6 %, respectively. It is worth mentioning that the maximum experiment uncertainty is estimated to be 8 %.

As there is no simple method for measuring the flow distribution through the microchannels and it needs a highly developed apparatus, to be confident about the model's another response parameter, flow distribution, an analytical model is generated for, U-type manifolds, by applying a few modifications to the original one presented in Wang [16]. Fig. 6 illustrates two small control volumes (cells) somewhere along the inlet and outlet manifolds and connected with a channel. For inlet manifold control volume, the conversation of mass is stated as:

$$\rho A_I V_I = \rho A_I \left(V_I + \frac{dV_I}{dX}\Delta X \right) + \rho A_C V_C \longrightarrow^{\Delta X = L/N} V_C = -\left(\frac{A_I}{A_C}\right)\left(\frac{L}{N}\right)\frac{dV_I}{dX} \tag{7}$$

In the above equation, as well as Fig. 6, V is velocity and A is cross-sectional area. Subscripts I and C represent inlet manifold and channel, respectively. Here, we use the fact that $\Delta X = L/N$. Where L and N are manifolds' length and system number of channels, respectively. Likewise, for outlet manifold we reach the following equation.

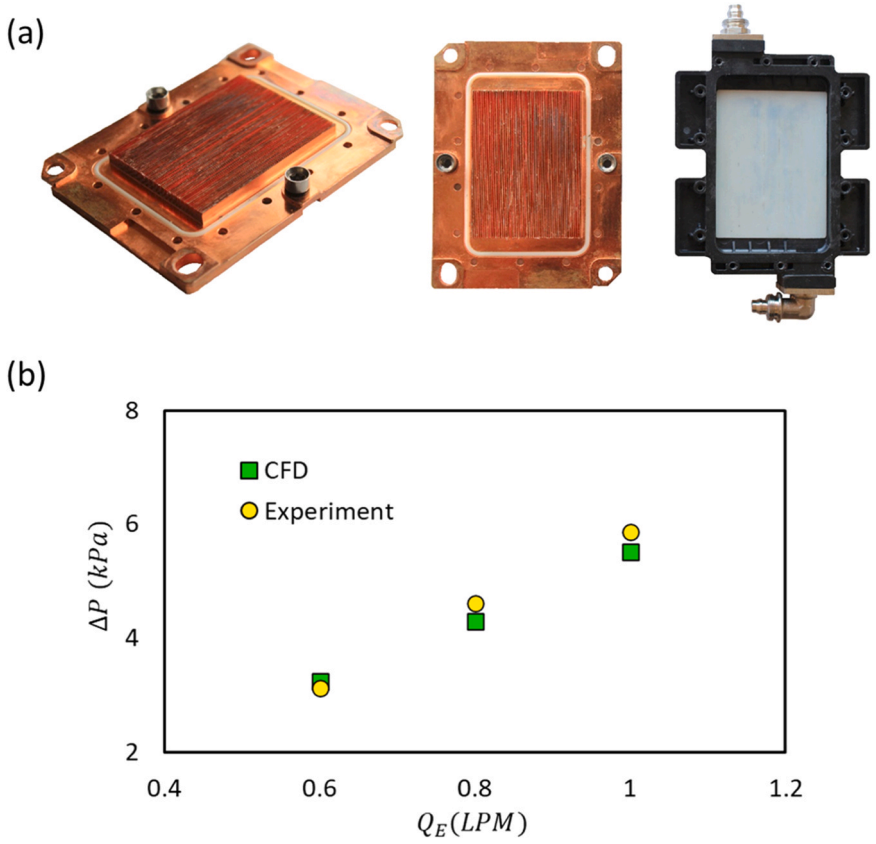

Fig. 5. Model methodology validation (a) the parallel channel water cooled heat sink with a Z-type manifold (b) comparison of numerical and experimental pressure drop data at three different flow rates.

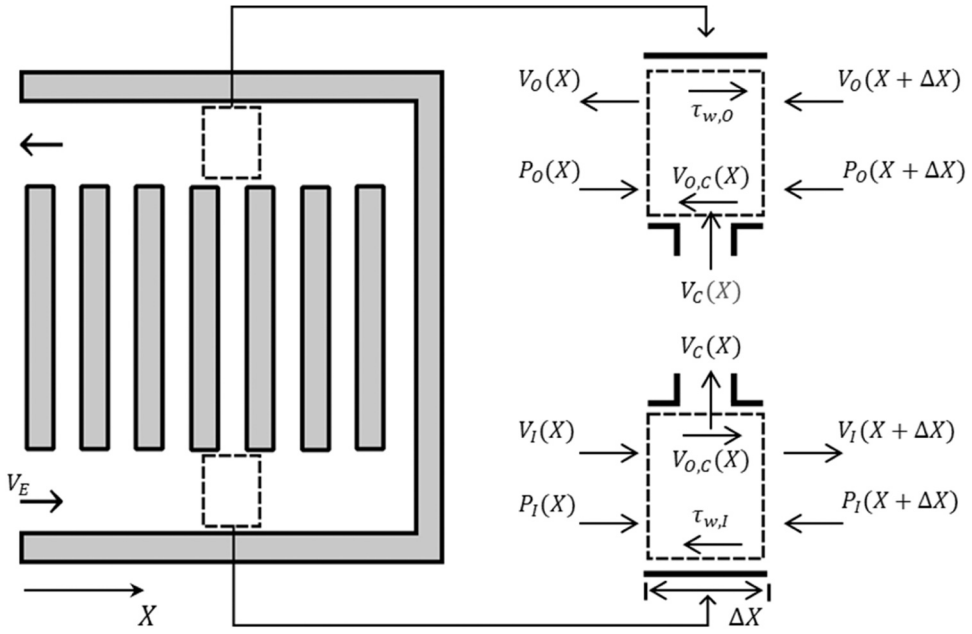

Fig. 6. Schematic of a U-type parallel channel system associated with control volumes in inlet and outlet manifolds used for developing the analytical model.

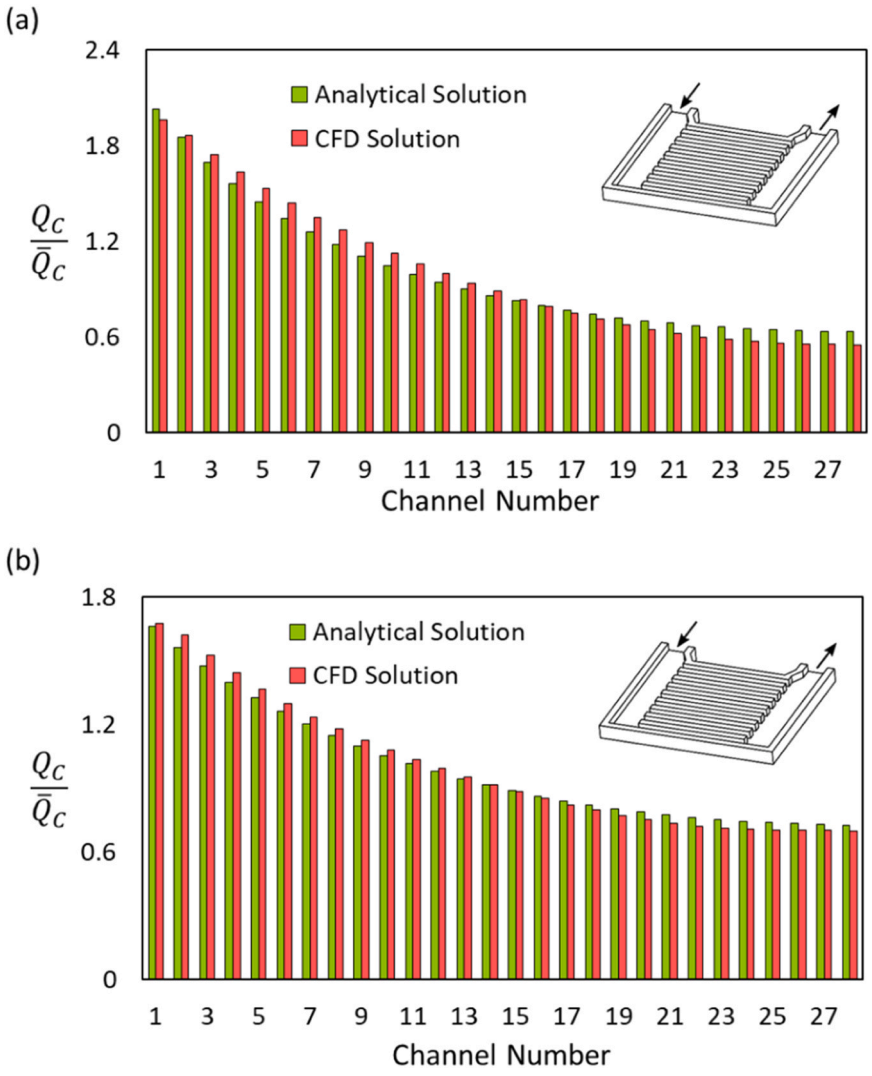

Fig. 7. Comparison of analytical and CFD solution for flow distribution through a U-type manifold system (a) at 1.5 LPM and (b) at 0.5 LPM total flow rate.

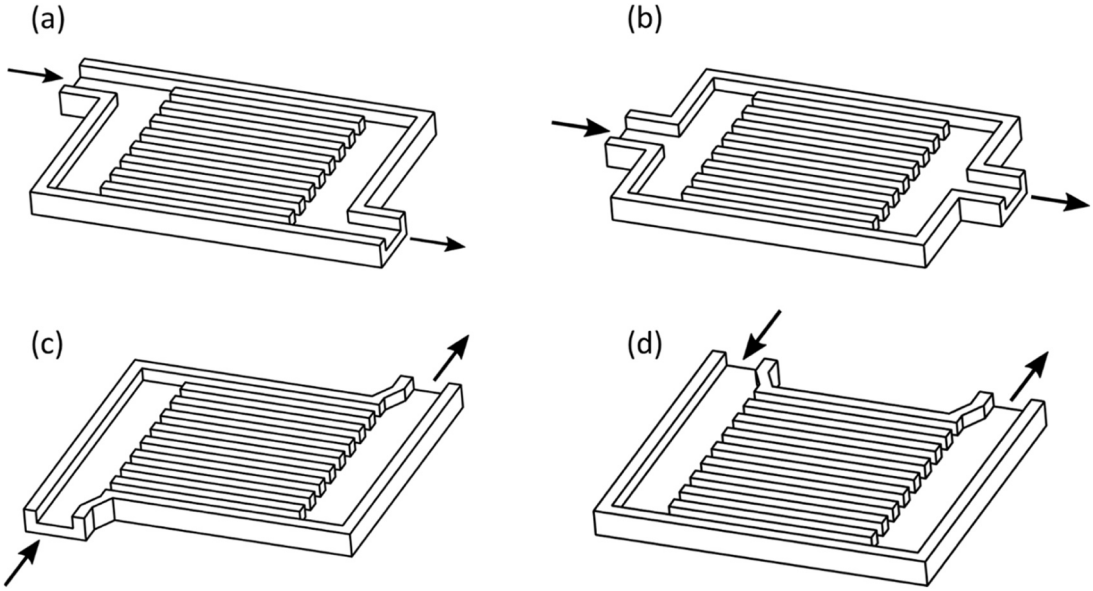

Fig. 8. The schematic of four basic common manifold designs (a) Z-type, (b) I-type, (c) N-type, and (d) U-type.

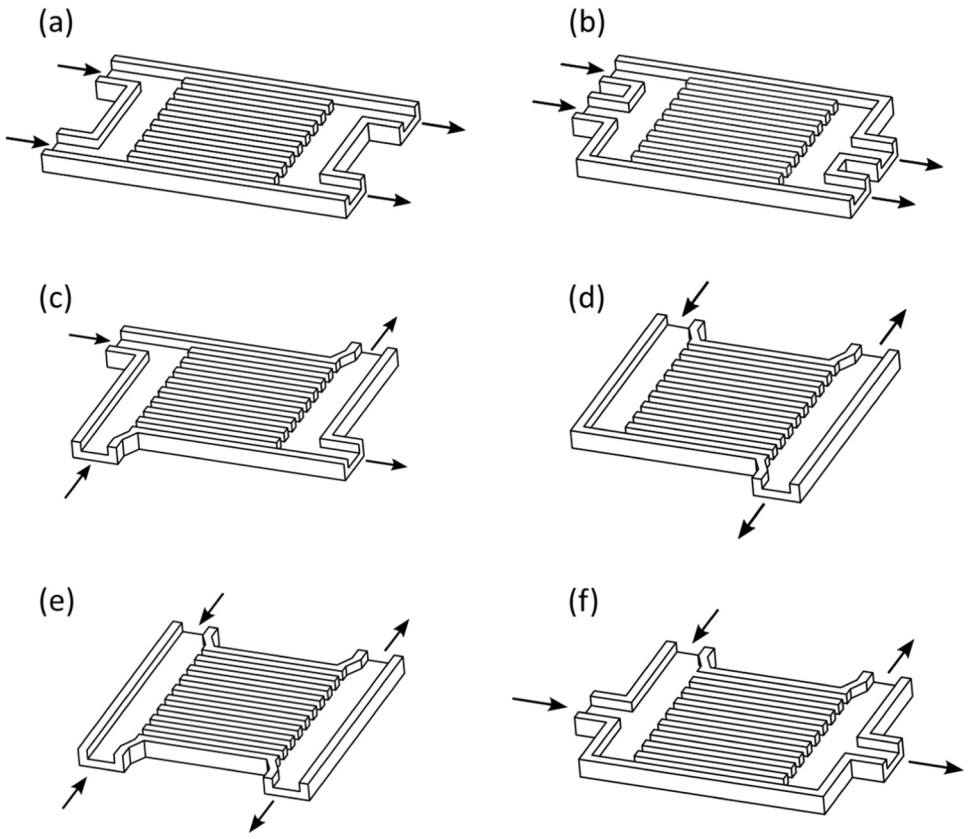

Fig. 9. The schematic of parallel combined manifold designs (a) Z+Z-type, (b) Z+I-type, (c) Z+N-type, (d) U+N-type, (e) U+U, and (f) U+I.

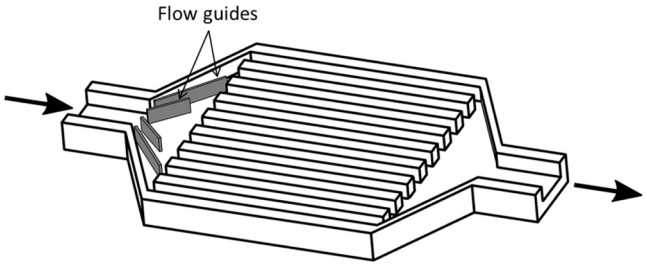

Fig. 10. Diffuser-Nozzle shaped manifolds with flow guides (blades).

$$V_C = -\left(\frac{A_O}{A_C}\right)\left(\frac{L}{N}\right)\frac{dV_O}{dX} \tag{8}$$

In the above equation the subscript *o* represents outlet manifold.

By applying the conservation of momentum to the inlet control volume we have:

$$P_I A_I - \left(P_I + \frac{dP_I}{dX}\Delta X\right)A_I - \tau_{w,I}\text{þ}_I \Delta X = \rho A_I\left(V_I + \frac{dV_I}{dX}\Delta X\right)^2 - \rho A_I {V_I}^2 + \rho A_C V_C V_{C,I} \tag{9}$$

In Eq. (9) P, τ_w, and þ denotes pressure, wall shear stress, and manifold cross-sectional perimeter, respectively. By using the definition of hydraulic diameter ($\frac{4A}{\text{þ}}$) and Darcy-Weisbach formula for τ_w:

$$\tau_{w,I} = \frac{1}{2}\rho f_I\left(\frac{V_I}{2}\right)^2 \tag{10}$$

as well as assuming $V_{C,I}$ is proportional to manifold mainstream velocity V_I

$$V_{C,I} = \beta_I V_I \tag{11}$$

Eq. (9) can be expresses as follows:

$$\frac{1}{\rho}\frac{dP_I}{dX} + \frac{f_I}{2D_{I,h}}{V_I}^2 + (2-\beta_I)V_I\frac{dV_I}{dX} = 0 \tag{12}$$

In the same way for outlet manifold we have:

$$\frac{1}{\rho}\frac{dP_O}{dX} - \frac{f_O}{2D_{O,h}}{V_O}^2 + (2-\beta_O)V_O\frac{dV_O}{dX} = 0 \tag{13}$$

Subtracting Eq. (13) from Eq. (12) we reach:

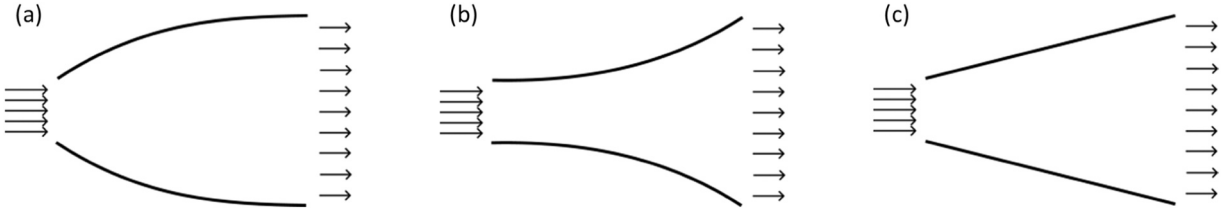

Fig. 11. Different shapes of diffuser (a) Bell shaped, (b) trumpet shaped, and (c) straight wall.

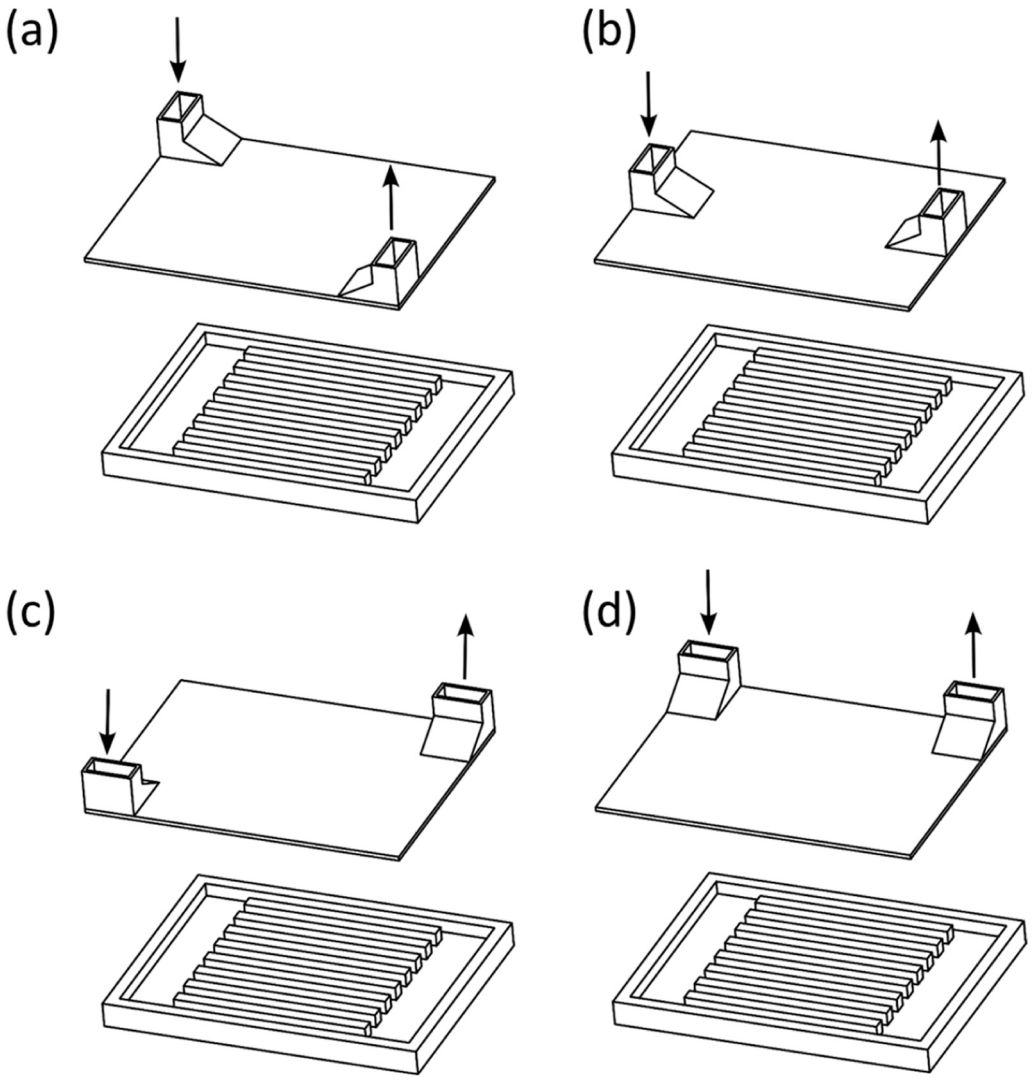

Fig. 12. The schematic of four basic vertical inlet-outlet manifold designs (a) VZ-type, (b) VI-type, (c) VN-type, and (d) VU-type.

$$\frac{1}{\rho}\frac{d(P_I-P_O)}{dX}+\frac{f_I}{2D_{I,h}}V_I{}^2+\frac{f_O}{2D_{O,h}}V_O{}^2+(2-\beta_I)V_I\frac{dV_I}{dX}-(2-\beta_O)V_O\frac{dV_O}{dX}=0 \tag{14}$$

Combining Eqs. (7) and (8) gives:

$$A_I dV_I = A_O dV_O \tag{15}$$

Taking integration from open ends of manifolds to an arbitrary channel we reach:

$$\int_{V_{I,I}}^{V_I} A_I dV_I = \int_{V_{O,O}}^{V_O} A_O dV_O \rightarrow A_I V_I - A_I V_{I,I} = A_O V_O - A_O V_{O,O} \tag{16}$$

In the above equation $V_{I,I}$ and $V_{O,O}$ are fluid velocity at the entrance of the inlet manifold and the exit of the outlet manifold, respectively. As both second terms at the left- and right-hand sides of Eq. (16) are equal to the system total flow rate, they cancel each other out.

$$V_O = \left(\frac{A_I}{A_O}\right)V_I \tag{17}$$

Substituting Eq. (17) in Eq. (14) we reach the following equation.

$$\frac{1}{\rho}\frac{d(P_I-P_O)}{dX}+(2-\beta_I)\left[1-\frac{(2-\beta_O)}{(2-\beta_I)}\left(\frac{A_I}{A_O}\right)^2\right]V_I\frac{dV_I}{dX}+\frac{1}{2}\left[\frac{f_I}{D_{I,h}}+\frac{f_O}{D_{O,h}}\left(\frac{A_I}{A_O}\right)\right]V_I{}^2=0 \tag{18}$$

Bernoulli's equation for a channel connecting our control volumes can be written as:

$$\frac{P_I}{\rho g}=\frac{P_O}{\rho g}+H_{loss} \tag{19}$$

Here, H_{loss} includes head losses due to friction along the channel and flow's change in direction at channel inlet and outlet.

$$H_{loss}=\left(k_{I,f}+k_{O,f}+f_C\frac{l_C}{D_{C,h}}\right)\frac{V_C{}^2}{2g} \tag{20}$$

In Eq. (20) $k_{I,f}$and $k_{O,f}$ are minor loss coefficients and can be expressed in terms on equivalent length and channel friction factor, f_C [43].

$$k_{I,f}=\frac{l_{I,e}}{D_{C,h}}f_C \tag{21}$$

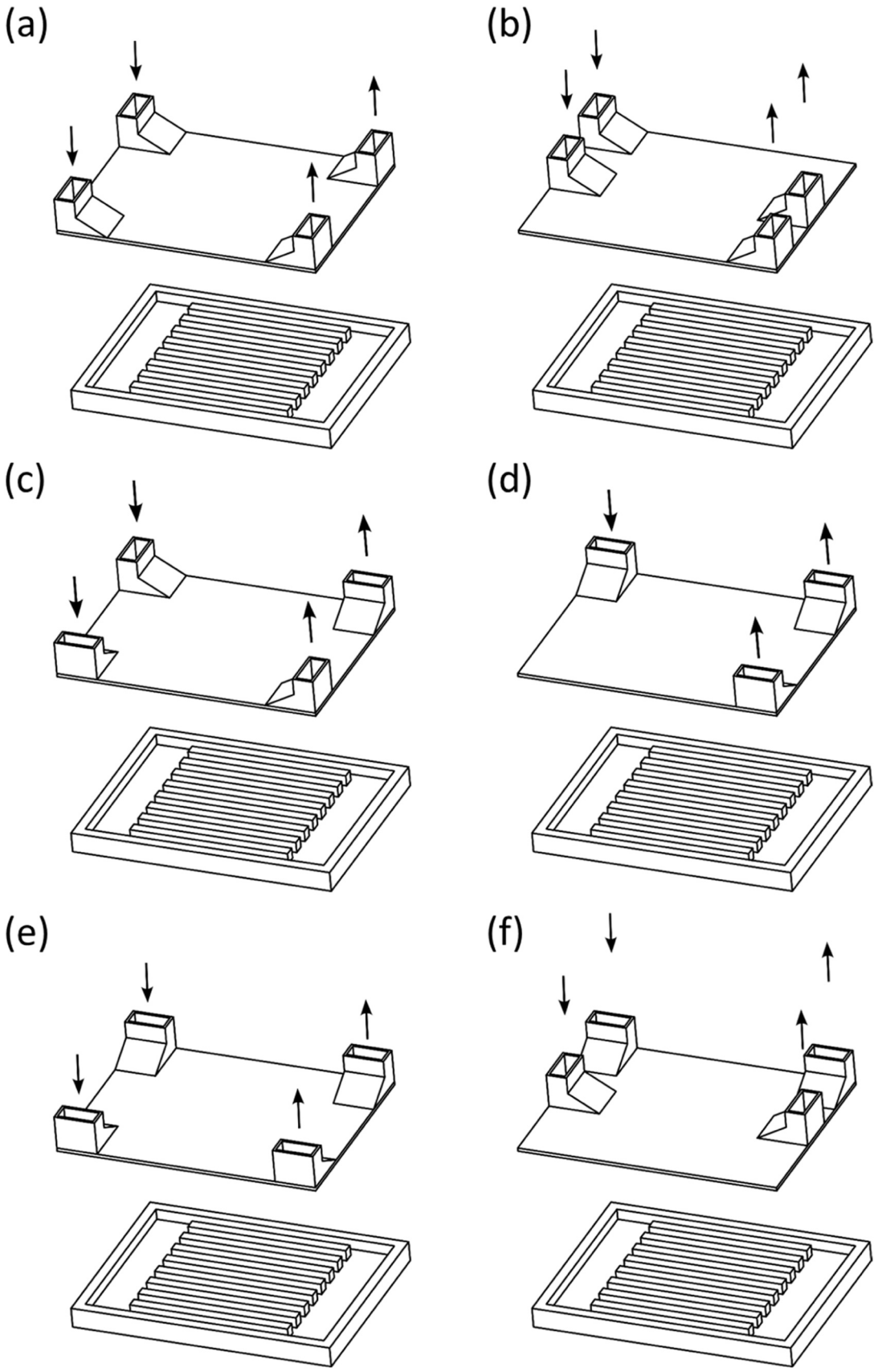

Fig. 13. The schematic of vertical combined manifold designs (a) VZ+VZ-type, (b) VZ+VI-type, (c) VZ+VN-type, (d) VU+VN-type, (e) VU+VU-type, and (f) VU+VI-type.

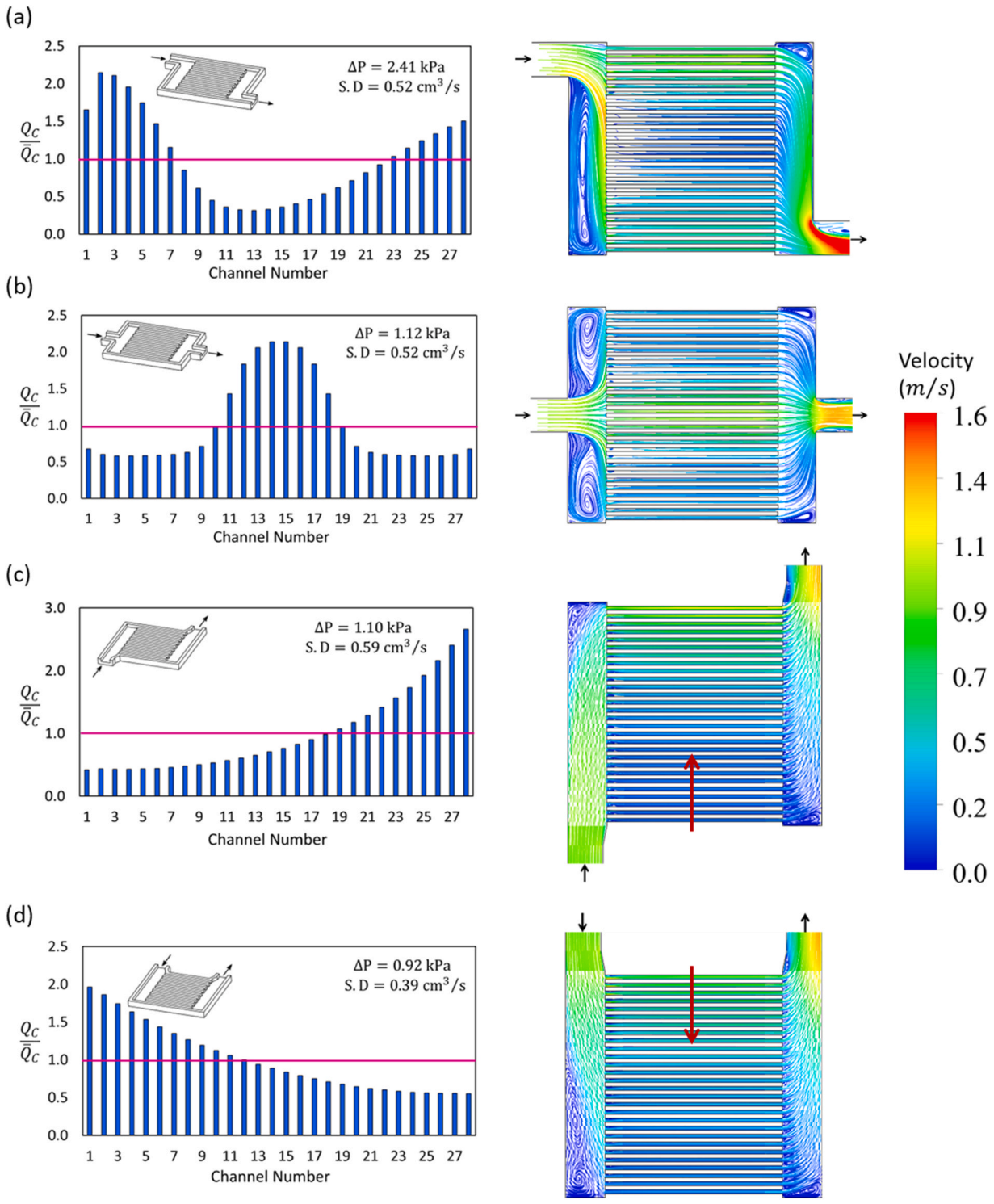

Fig. 14. Four parallel conventional manifold designs, flow distribution and pattern (a) Z-, (b) I-, (c) N-, and (d) U-type.

$$k_{I,f} = \frac{l_{O,e}}{D_{C,h}} f_C \tag{22}$$

Friction factor can be expressed in the following general form for laminar and turbulent flow.

$$f = \frac{\Psi}{\mathrm{Re}_{D_h}{}^{n}} \tag{23}$$

Where Re_{D_h} is flow Reynolds number and Ψ is duct's shape factor depending on its cross-sectional area. With the assumption of laminar flow through channels $n = 1$. Substituting Eqs. (23), (22) and (21) in (20) and extending channel Reynolds number yields:

$$H_{loss} = \zeta \frac{\Psi_{C\nu}}{D_{C,h}} \frac{V_C}{2g} \tag{24}$$

In Eq. (24) ζ is a geometric parameter expressed as:

$$\zeta = \frac{l_{I,e}}{D_{C,h}} + \frac{l_{O,e}}{D_{C,h}} + \frac{l_C}{D_{C,h}} \tag{25}$$

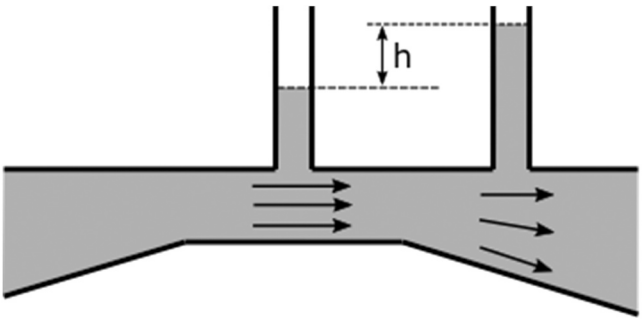

Fig. 15. Venturi effect, a change in velocity causes pressure difference in vertical tubes.

For fully developed laminar flow through rectangular channels Ψ is expressed as ([44]):

$$\Psi_C = \frac{96}{\left(1+\frac{w_C}{d_C}\right)^2\left[1-\frac{192}{\pi^5}\left(\frac{w_C}{d_C}\right)\tanh\left(\frac{\pi}{2}\frac{d_C}{w_C}\right)\right]} \tag{26}$$

Inserting Eq. (24) in Eq. (19) and rearranging it we have:

$$P_I - P_O = \frac{1}{2}\rho\zeta\frac{\Psi_C\nu}{D_{C,h}}V_C \tag{27}$$

Replacing V_C in Eq. (27) with Eq. (7) yields:

$$P_I - P_O = -\frac{1}{2}\rho\zeta\frac{\Psi_C\nu}{D_{C,h}}\left(\frac{A_I}{A_C}\right)\left(\frac{L}{N}\right)\frac{dV_I}{dX} \tag{28}$$

Inserting Eq. (28) in Eq. (18) we have:

$$-\frac{1}{2}\zeta\frac{\Psi_C\nu}{D_{C,h}}\left(\frac{A_I}{A_C}\right)\left(\frac{L}{N}\right)\frac{d^2V_I}{dX^2}+\frac{1}{2}\left[\frac{f_I}{D_{I,h}}+\frac{f_O}{D_{O,h}}\left(\frac{A_I}{A_O}\right)\right]V_I{}^2+(2-\beta_I)\left[1-\frac{(2-\beta_O)}{(2-\beta_I)}\left(\frac{A_I}{A_O}\right)^2\right]V_I\frac{dV_I}{dX}=0 \tag{29}$$

Defining dimensionless inlet manifold velocity and space coordinate,

$$v_I = \frac{V_I}{V_E} \tag{30}$$

$$x = \frac{X}{L} \tag{31}$$

Eq. (29) can be nondimensionalized as follows:

$$-\frac{1}{2}\zeta\frac{\Psi_C\nu}{D_{C,h}V_E}\left(\frac{A_I}{A_CN}\right)\frac{d^2v_I}{dx^2}+\frac{1}{2}\left[\frac{f_I}{D_{I,h}}+\frac{f_O}{D_{O,h}}\left(\frac{A_I}{A_O}\right)\right]v_I{}^2+(2-\beta_I)\left[1-\frac{(2-\beta_O)}{(2-\beta_I)}\left(\frac{A_I}{A_O}\right)^2\right]v_I\frac{dv_I}{dx}=0 \tag{32}$$

In Eq. (30), V_E is the system inlet velocity (Fig. 6). Unlike in mini/microchannels, flow could be partially turbulent in manifolds. Using Eq. (23) inlet and outlet manifolds friction factors (f_I & f_O) can be obtained as follows:

$$f_I = \frac{\Psi_I}{\left(\frac{V_ID_{I,h}}{\nu}\right)^n} = \frac{\Psi_I}{\left(\frac{V_ED_{I,h}}{\nu}\right)^n}v_I{}^{-n} = \frac{\Psi_I}{(\mathrm{Re}_{I,E})^n}v_I{}^{-n} \tag{33}$$

Using Eqs. (17) and (30) we have:

$$f_O = \frac{\Psi_O}{\left(\frac{V_OD_{O,h}}{\nu}\right)^n} = \frac{\Psi_O}{\left[\left(\frac{A_I}{A_O}\right)\frac{V_ID_{O,h}}{\nu}\right]^n} = \frac{\Psi_O}{\left[\left(\frac{A_I}{A_O}\right)\frac{V_ED_{O,h}}{\nu}\right]^n}v_I{}^{-n} = \frac{\Psi_O}{\left(\frac{A_I}{A_O}\right)^n(\mathrm{Re}_{O,E})^n}v_I{}^{-n} \tag{34}$$

In Eqs. (33) and (34), $\mathrm{Re}_{I,E}$ ($\frac{V_ED_{I,h}}{\nu}$) and $\mathrm{Re}_{O,E}$ ($\frac{V_ED_{O,h}}{\nu}$) are inlet and outlet manifolds Reynolds numbers based on the system inlet velocity and are fixed for a specified system. By substituting Eq. (33) and Eq. (34) in Eq. (32) and rearranging it, we reach:

$$\frac{d^2v_I}{dx^2} - Av_I\frac{dv_I}{dx} - Bv_I{}^{2-n} = 0 \tag{35}$$

With boundary conditions of:

$$v_I(0) = 1 \tag{36}$$

$$v_I(1) = 0 \tag{37}$$

Here,

$$A = \frac{2\mathrm{Re}_{C,E}}{\Psi_C\zeta}\left(\frac{A_CN}{A_I}\right)(2-\beta_I)\left[1-\frac{(2-\beta_O)}{(2-\beta_I)}\left(\frac{A_I}{A_O}\right)^2\right] \tag{38}$$

$$B = \frac{\mathrm{Re}_{C,E}}{\Psi_C\zeta}\left(\frac{A_CN}{A_I}\right)\left[\frac{\Psi_IL}{D_{I,h}}\left(\frac{1}{\mathrm{Re}_{I,E}}\right)^n+\frac{\Psi_OL}{D_{O,h}}\left(\frac{1}{\mathrm{Re}_{O,E}}\right)^n\left(\frac{A_I}{A_O}\right)^{1-n}\right] \tag{39}$$

$$\mathrm{Re}_{C,E} = \frac{D_{C,h}V_E}{\nu} \tag{40}$$

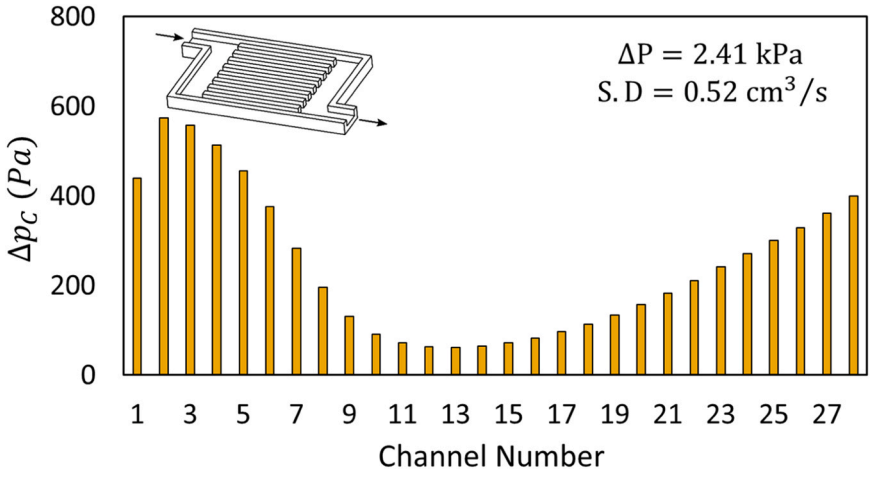

Fig. 16. Channel pressure drop for system with parallel Z-type manifold, channel pressure drop follows the same trend of channel flow rate.

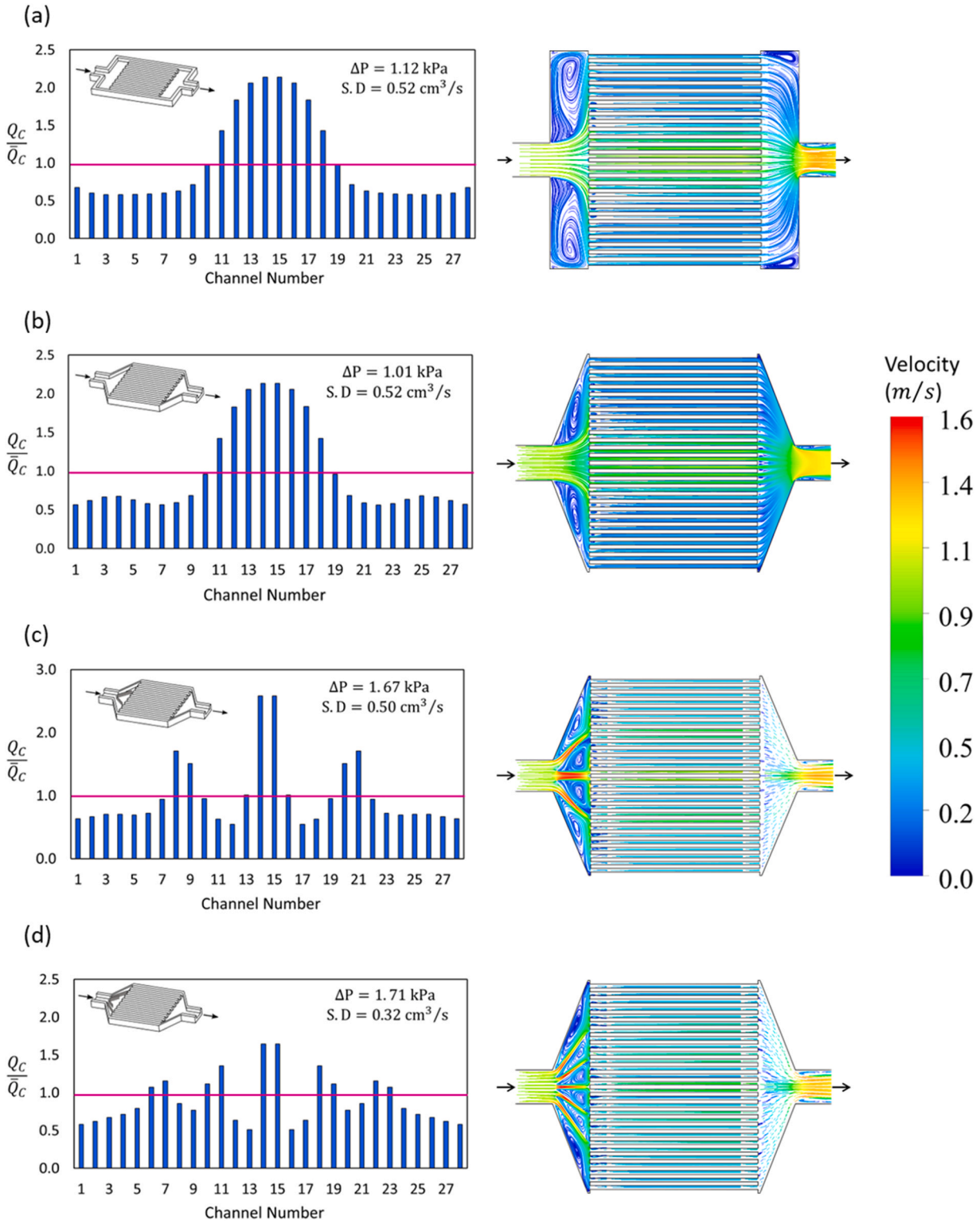

Fig. 17. Flow distribution and pattern in the class of the I-type manifold (a) original I-type, (b) diffuser-shaped, (c) diffuser-shaped with two guide vanes and (d) diffuser-shaped with four guide vanes.

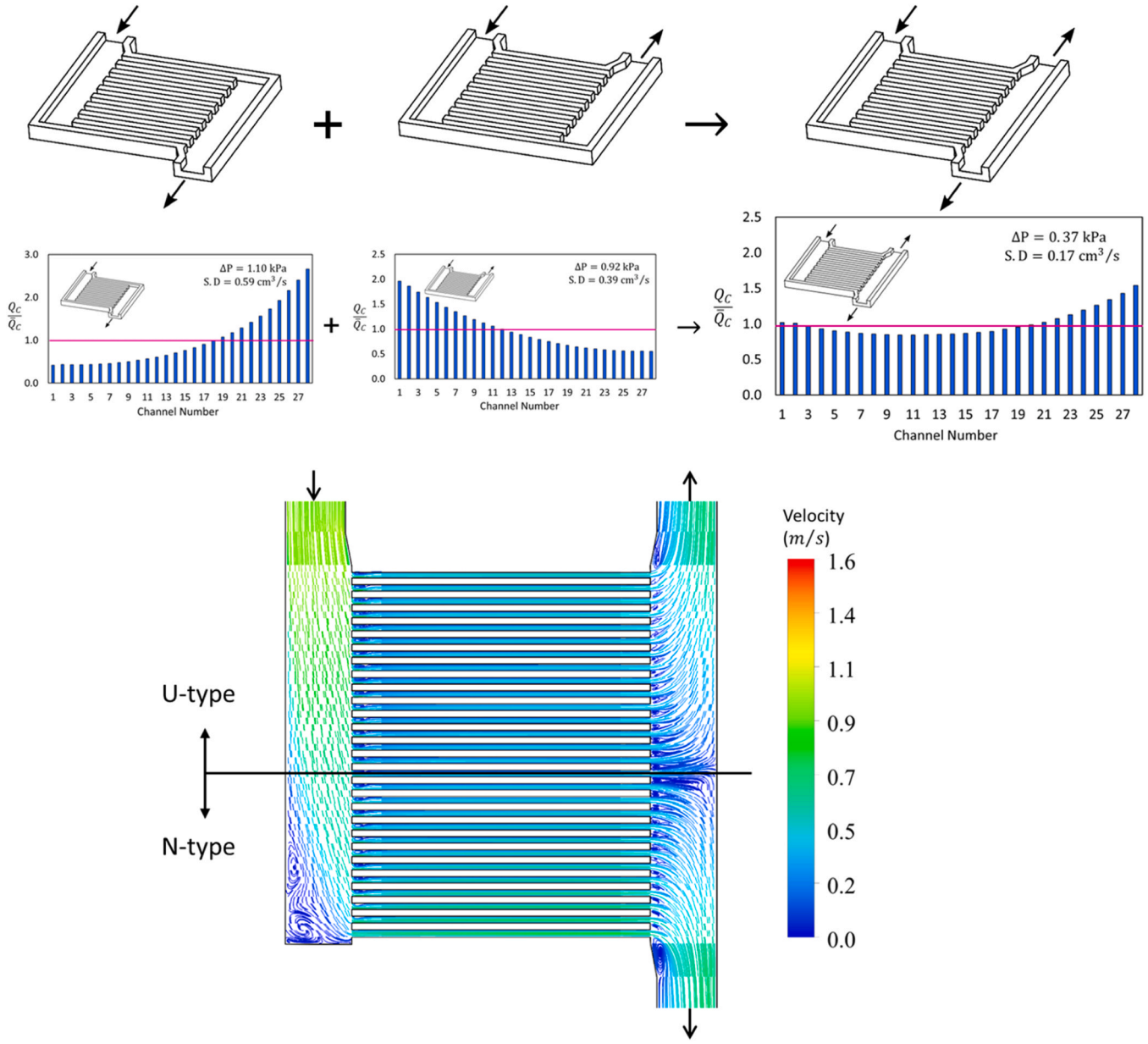

Fig. 18. Combination of N-type and U-type manifolds with a same inlet duct, flow distribution and pattern.

$\Psi_{I/O}$ can be expressed in form of a piecewise function for laminar and turbulent flow [44,45].

$$\Psi_{I/O} = \begin{cases} \dfrac{96}{\left(1+\frac{w_{I/O}}{d_{I/O}}\right)^2\left[1-\frac{192}{\pi^5}\left(\frac{w_{I/O}}{d_{I/O}}\right)\tanh\left(\frac{\pi}{2}\frac{d_{I/O}}{w_{I/O}}\right)\right]} \text{Laminar} \\ \dfrac{0.3068}{\left(\frac{w_{I/O}+d_{I/O}}{2\sqrt{w_{I/O}d_{I/O}}}\right)^{0.25}} \text{Turbulent} \end{cases} \quad (41)$$

In Eq. (35) $n = 1$ is for laminar flow and $n = \frac{1}{4}$ for turbulent flow.

To have a validation based on the channel flow distribution, Eq. (35) is solved numerically, and the results are compared with CFD results for U-type manifold. Fig. 7 compares the solutions of flow distribution at 0.5 (when flow is laminar everywhere) and 1.5 LPM.

In Fig. 7, Q_C and $\overline{Q}_C$ denote channel and channel average ($\frac{Q_E}{N}$) flow rate, respectively. As Fig. 7 shows analytical and CFD results are in good agreement. The maximum and average discrepancies are 15 % and 7 % for the flow rate of 1.5LPM and 6 % and 3 % for 0.5 LPM, respectively.

4. Designs examined

4.1. Parallel inlet-outlet designs

The designs studied in this study, are categorized to designs in which flow enters and exits the system parallel and vertical to the channels plane. Flow distribution and pressure drop in four basic parallel manifold (Z-, I-, N-, and U-type) which are widely used in different industrial applications, are studied. Fig. 8 shows the schematic of these four designs. As it can be seen in Fig. 8, in Z-type and I-type manifolds flow enters and exits in the direction of channels while in N-type and Z-type manifolds, flow enters and exits the system perpendicular to the direction of channels. Multi-inlet/outlet combinations of these four basic designs are developed based on their results. The purpose of combining the elementary designs is to reach designs with more uniform flow

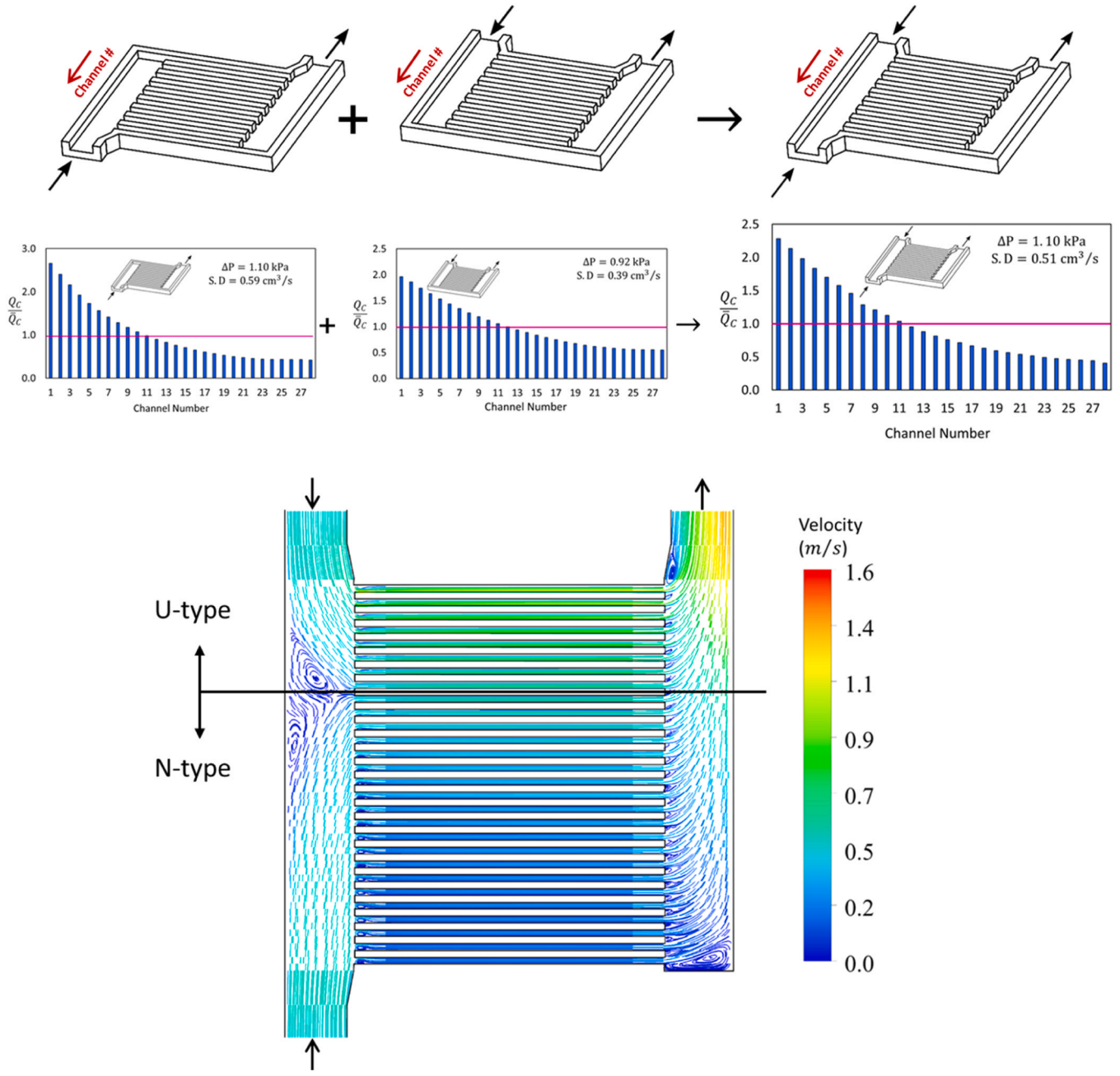

Fig. 19. Combination of N-type and U-type manifolds based on the same outlet, flow distribution and pattern.

distribution and lower pressure drop. Fig. 9 shows the schematics of six of the combined parallel designs.

In the I-type manifolds flow experiences a sudden expansion and contradiction along its path from the inlet duct to the distributor and from collector to outlet duct, respectively. According to fundamentals of fluid dynamics, [46,47], it is expected that, the performance of a regular I-type manifold improves by making this expansion and contraction moderate as much as possible. To do so, the I-type manifolds distributor and collector can be transferred from rectangular to diffuser and nozzle shaped, respectively (Fig. 10). Diffusers are diverging ducts widely used in fluid dynamics to recover pressure along the flow. They are designed and optimized to remain unstalled and deliver flow uniformly, as much as possible, at their outlets. Based on their geometry, diffusers are categorized to bell-shaped, trumpet-shaped, and straight-wall. Fig. 11 demonstrates three different diffuser shapes. A bell-shaped diffuser has an initial divergence angle typically twice of the straight-wall diffuser and a final divergence angle of zero, whereas the trumpet-shaped diffuser has an initial divergence angle of zero and an outlet divergence angle of commonly double of straight-wall diffuser. While bell-shaped and trumpet-shaped have their specific advantages in enhance mixing, dispersion, and flow direction in particular applications [48], straight-wall diffusers offer a combination of uniform flow distribution, simpler design, simpler manufacturing process, and cost-effectiveness. These advantages make straight-wall diffusers a preferred choice for parallel channel systems manifold. The main design parameters for diffusers, are area ratio (A_{out}/A_{in}), which is the ratio of the diffuser's outlet area to inlet area, and divergence angle. Flow guides (blades) are used to prevent stall phenomenon and improve the performance when working with short and large divergence angle diffusers [48]. The idea of employing straight wall diffuser and nozzle geometries for I-type manifolds distributor and collector is used in this study to investigate whether an enhancement occurs in the system performance.

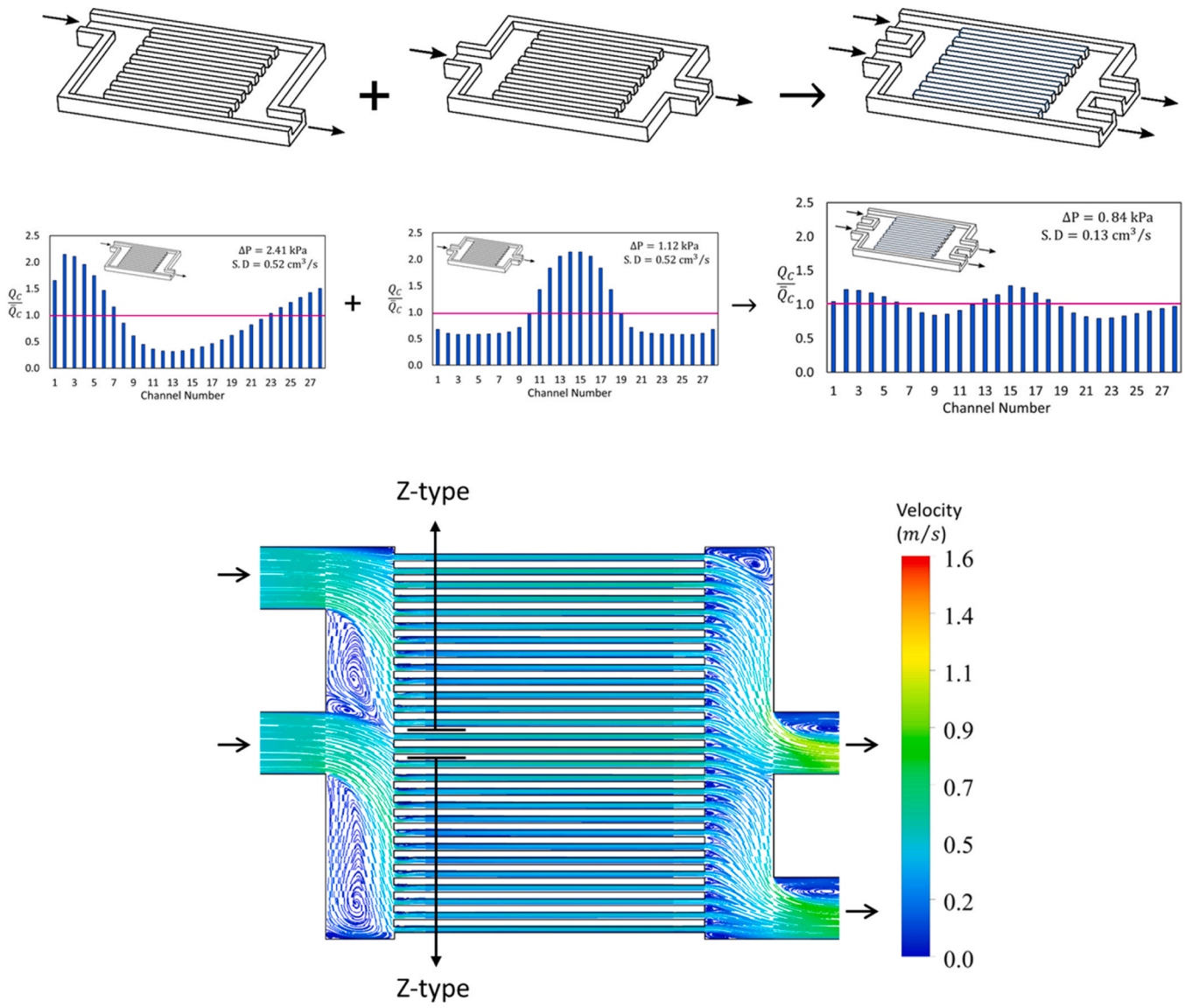

Fig. 20. Combination of Z-type and I-type manifolds, flow distribution and pattern.

Flow guides are used in the distributor to enhance flow distribution uniformity. It is shown that the performance of the system is strongly affected by the number and position of the flow guides. Fig. 10 illustrates diffuser-nozzle shaped manifolds with associated flow guides in the distributor. An algorithm for calculating the optimal number, position, direction, and length of the flow guides for diffusers with various area ratio and divergence angle has been presented in [48].

4.2. Vertical inlet-outlet designs

System performance (pressure drop and flow distribution uniformity) are strongly affected by flow pattern through inlet and outlet ducts and manifolds. Changing the inlet and outlet ducts direction from parallel into vertical to the channel network, significantly influences flow field in manifolds. To have an estimation of vertical inlet and outlet designs, like parallel designs, different vertical designs and their combinations are solved for the same channel network. Fig. 12 shows the four basic vertical inlet-outlet designs. As the system inlet and outlet cross sectional area ($3 \times 9mm$) is fixed along the whole study, the vertical ducts are designed to gradually change the width from $3mm$ to $10mm$ (width of manifolds, w_M) along the lower half of their height. As Fig. 12 shows, like parallel designs, in vertical Z-type and I-type manifolds, flow is conducted parallel to channels by the inlet ducts. In vertical N-type and U-type manifolds, inlet ducts direct flow along the length of distributor as in parallel designs. Multi-inlet/outlet combinations of the four basic designs are developed based on their results as is done for parallel designs. The purpose of combining the elementary designs is to reach designs with more uniform flow distribution and lower pressure drop. Fig. 13 shows the schematics of six combined vertical designs.

5. Results and discussion

5.1. Basic parallel designs

The results of flow pattern (streamlines) and distribution for the four basic parallel channel manifolds are shown in Fig. 14. It should be mentioned that in all figures in this study channels are counted by getting far from the inlet except for the I-type manifolds. As I-type manifolds are symmetric, channels are counted from one side to the other side of the channel network. Pressure drop and flow distribution standard deviation, as a measure of flow uniformity, are mentioned on the flow distribution charts. There are four factors which determine flow pattern and distribution inside the systems. These factors can be listed as:

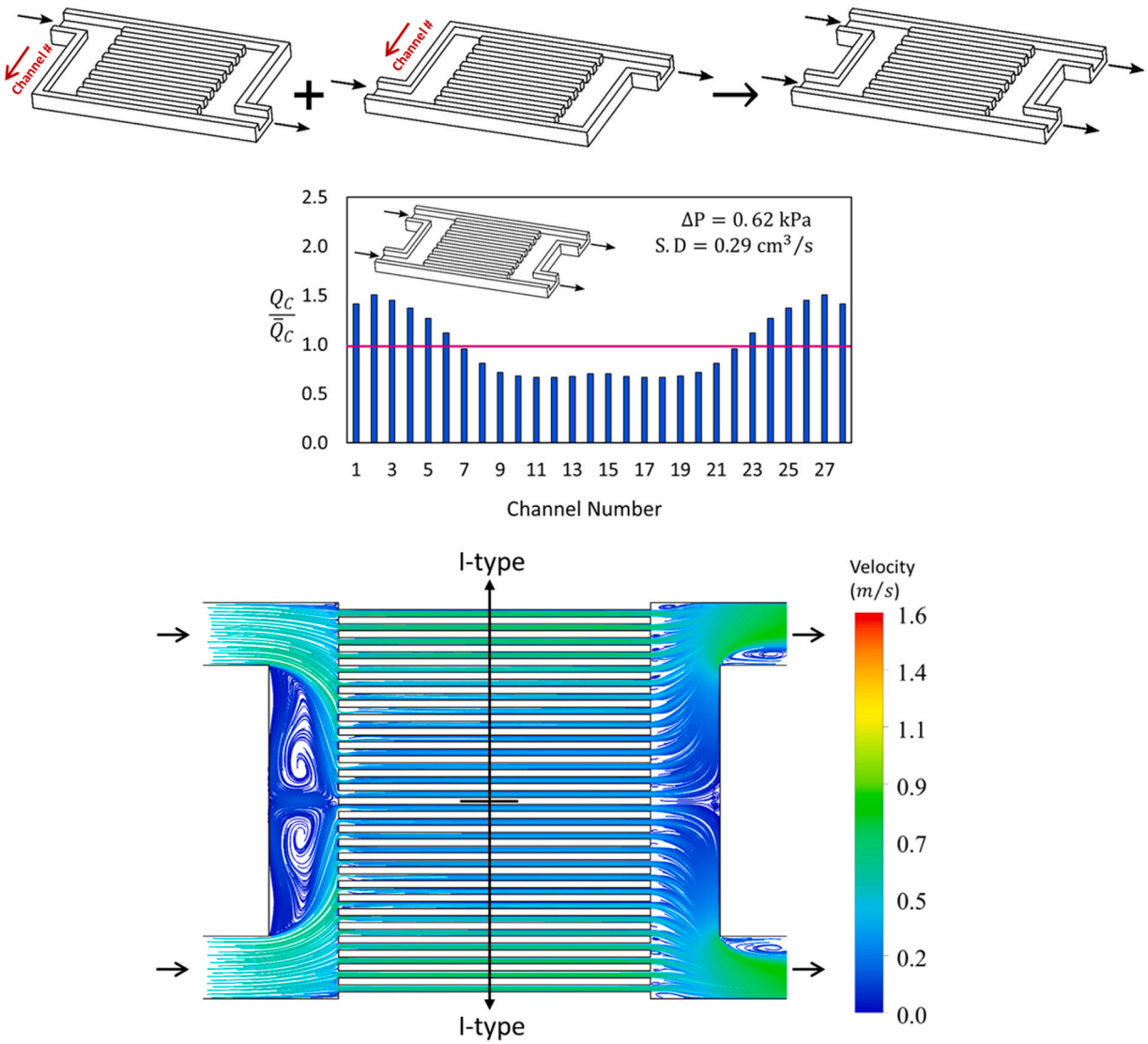

Fig. 21. Combination of two Z-type manifolds, flow distribution and pattern.

momentum effects (charge of momentum through the inlet and discharge of it through the outlet) flow path through the system, and Bernoulli induced pressure (Venturi effect). The factor of momentum effect represents the channel pressure drop caused by inlet's flow supply or outlet's flow suction where inlet and outlet flows are in the direction of channels (Z-type and I-type). It should be noted that inlet and outlet flows mainly affect the channels which are in front of them, and their effects decrease by getting far from them. The Venturi effect occurs where two flows are perpendicular and the change in the velocity of one of them causes change in pressure of the other one according to Bernoulli's law. Fig. 15 shows the Venturi effect and how a change in flow velocity results in vertical ducts' pressure difference.

Fig. 14(a) shows the flow pattern and distribution of the case with Z-type manifolds. As can be seen, channels close to inlet and outlet benefit from their momentum effects and receive more flow than the channels in the middle which are far from the inlet and outlet ducts. The horizontal solid pink line on the flow distribution charts shows ideal scenario of uniform flow distribution with the same flow rate (1.5 LPM).

Fig. 14(b) illustrates the flow pattern and distribution for a system of parallel channels with I-type manifolds. As it is expected, channels in the middle receive more flow rate as they are between the inlet and outlet ducts. They also provide shorter flow paths (lower flow resistance) than the channels far from inlet and outlet ducts and closer to the sides.

Fig. 14(c) shows flow pattern and distribution created by N-type manifolds. As the figure shows, channel flow rate increases monotonically by getting away from the inlet (in the direction of red arrow). As opposed to Z-type manifolds, N-type manifolds conduct the flow perpendicular to the channels and do not supply the fluid into or suction the fluid from the channels directly. In N-type distributer, flow velocity monotonically decreases by getting away from inlet duct, due to branching, which results in a monotonic increase in channels' inlet pressure according to Bernoulli's law (Fig. 15). The reverse occurs in the collector, as the flow velocity increases by approaching the outlet duct due to merging, channels' outlet pressure decreases toward it. This increase in channels inlet pressure and decrease in channels outlet pressure, by getting away from inlet duct, results in an ascending channel pressure drop with distance from inlet duct that leads to a same trend for flow distribution.

The flow pattern and distribution of the system with U-type manifolds are shown in Fig. 14(d). In this case unlike N-type manifolds, both inlet and outlet ducts are in the one side of the channel network. Channels outlet pressure follows the same trend as in N-type. Here, like in N-type's collector the flow velocity increases by approaching the outlet duct. Therefore, channels outlet pressure decreases by approaching outlet. In the distributor, however, the velocity decreases by getting away from the inlet duct which results in monotonic increase

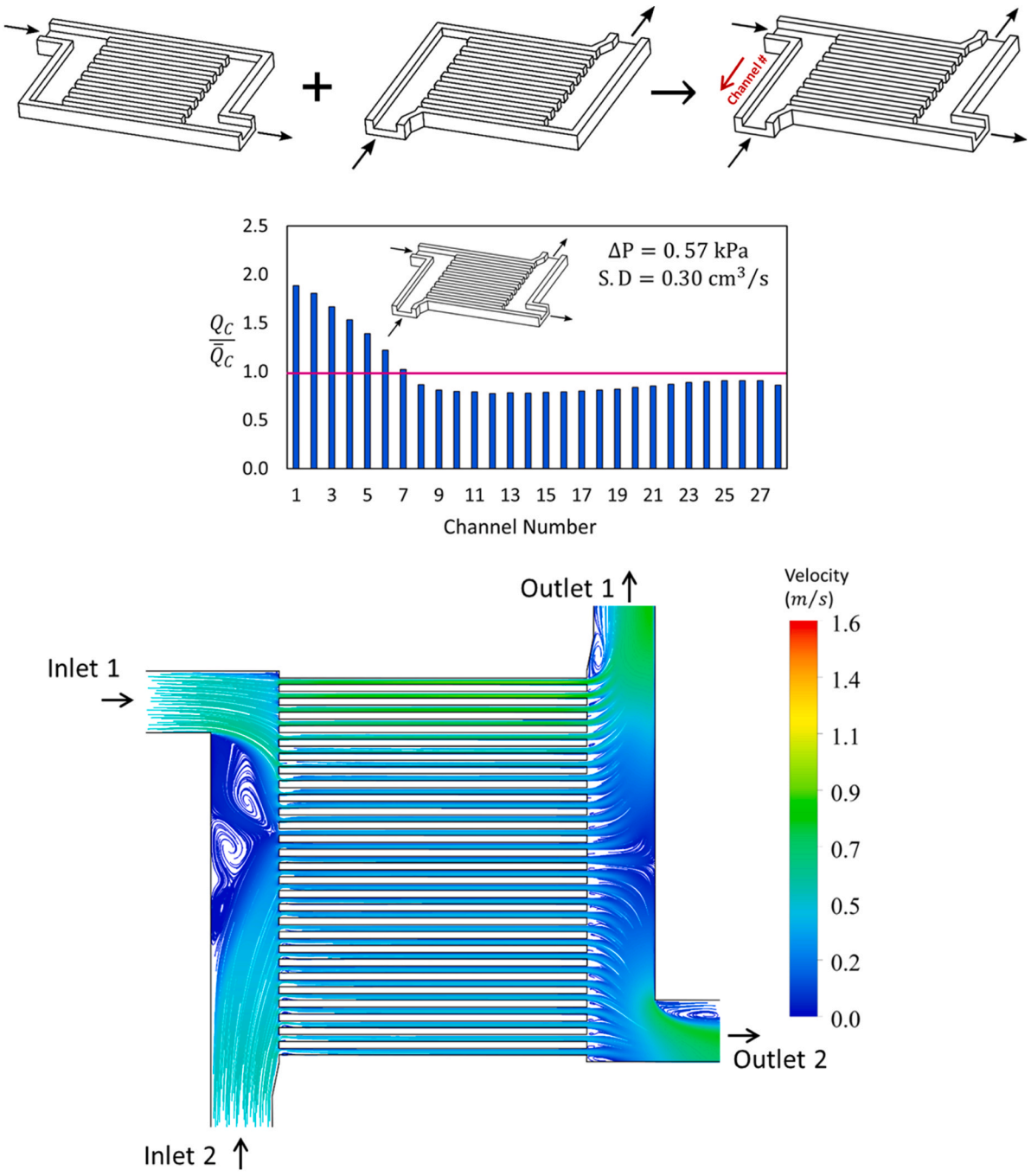

Fig. 22. Combination of Z-type and N-type manifolds, flow distribution and pattern.

in channel inlet pressure. In other words, in U-type manifolds, channel both inlet and outlet pressures increase by getting distance from inlet duct (in the direction of red arrow) which bring channels in milder pressure drop than in N-type manifolds. U-type manifolds provide more uniform flow because they provide more uniform channel pressure drop as in the collector, outlet pressure of the channels with higher inlet pressure increases. Moreover, U-type manifolds offer shorter flow path to the channels closer to their inlet and outlet ducts and cause more flow travels through them.

Comparing the pressure drop of four basic cases, we find that the pressure drop of the Z-type system is significantly higher than the others. As Fig. 14(a) shows a big eddy is formed in the outlet of Z-type manifold which blocks almost half of the outlet duct's area. By blocking half of the exit area, the eddy increases the outlet velocity resulting in the outlet pressure reduction and system higher total pressure drop. Although the pressure drop is almost the same in systems with I-type and N-type manifolds, I-type manifold offers slightly more uniform flow distribution than N-type manifold. The results show that among the four designs, U-type manifold provides lowest pressure drop and most uniform flow distribution as it exerts most uniform pressure on channels inlet and outlet.

It is worth noting that, based on the energy equation, channel flow rate follows the same trend of channel pressure drop. In other words, channels with higher pressure difference transfer higher amount of fluid. Fig. 16 shows the calculated pressure drop through the channels for system with Z-type manifolds. As it is expected, channel pressure drop possesses the same trend of flow distribution (Fig. 14(a)).

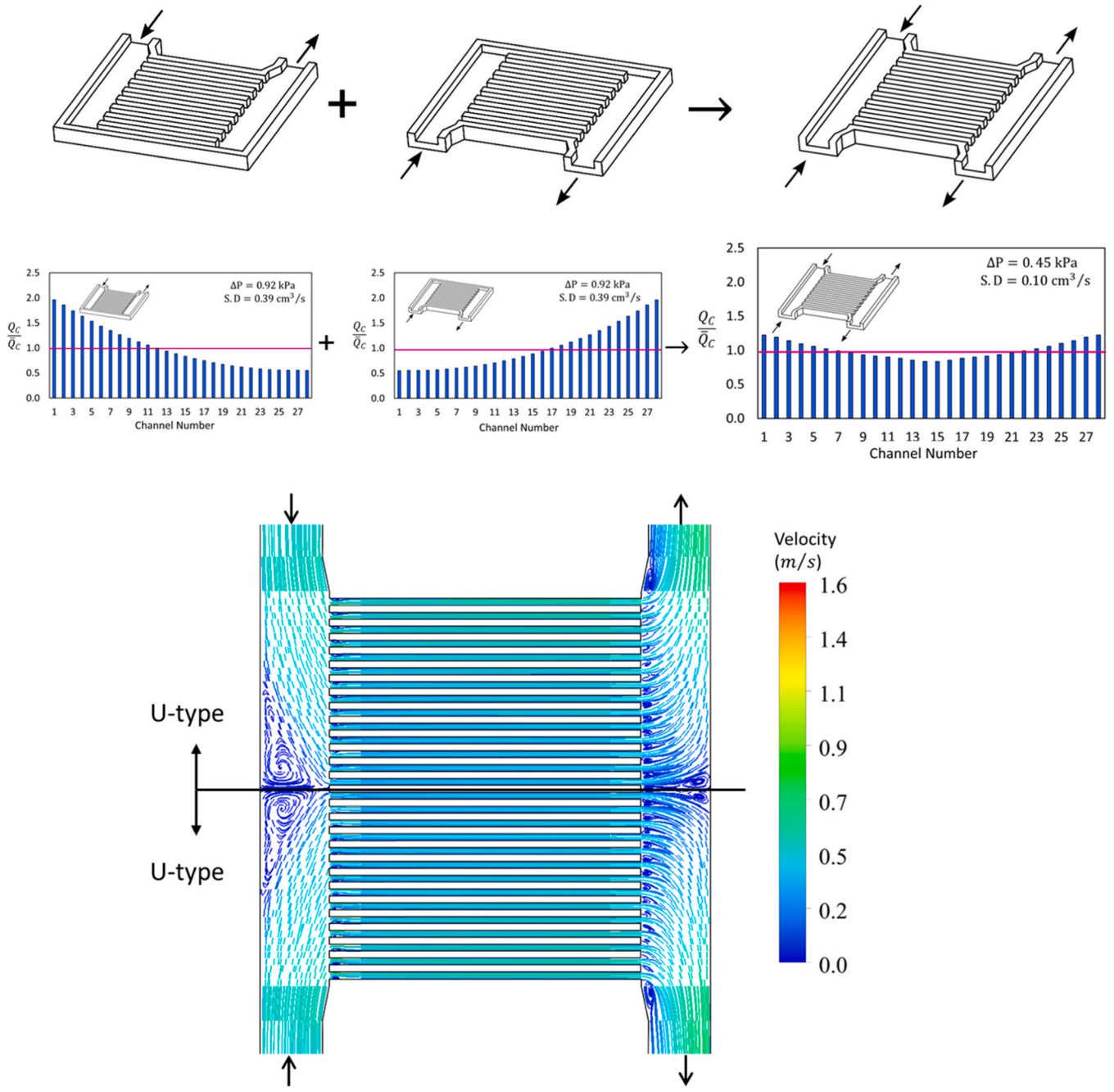

Fig. 23. Combination of two reflective U-type manifolds, flow distribution and pattern.

5.2. *Diffuser-nozzle I-type manifolds.*

Fig. 17 compares flow distribution and pattern of the original I-type manifold with diffuser-nozzle shaped manifolds with and without guide vanes. As can be seen, from original I-type manifold (Fig. 17(a)) to diffuser-nozzle shaped manifold (Fig. 17(b)) flow uniformity distribution (flow standard deviation) does not change significantly as in both cases middle channels benefit the momentum effects of inlet and outlet and provide paths with lower flow resistance than channels far from inlet and outlet ducts (close to sides). The result shows a slight reduction in pressure drop of 10 %. In diffuser-shape distributor the large eddies shrink significantly which leads to less flow energy loss. Two small eddies in the collector of the original I-type manifold (Fig. 17(a)) are also removed by nozzle-shape collector (Fig. 17(b)).

In Fig. 17(c), two guide vanes are added to the distributor with the idea of deviating parts of the flow to the channels far from middle. Indeed, by adding guide vanes, one splits the distributor diffuser to sub-diffusers with lower divergence angle. The location and geometrical dimensions of the guide vanes are calculated based on an instruction of optimal vane arrangement presented in [47] and then modified by trial and error using computational modeling. As can be seen in Fig. 17(c) two guide vanes divide the distributor to three sub-diffusers with three jets. A high-velocity jet is formed in the center of the middle sub-diffuser, due to its big divergence angle, that supply more flow to the channels next to it (channels Nos. 14 and 15). Two jets are formed in the side sub-diffuses closer to the guide vanes due to their asymmetric geometry. These jets also direct more flow to the channels close to themselves (channels Nos. 8, 9, 20, and 21). The bell-shaped flow distribution of diffuser-nozzle shaped manifold (Fig. 15(b)) is totally disarranged by adding the guide vanes. Although adding two guide vanes to the diffuser

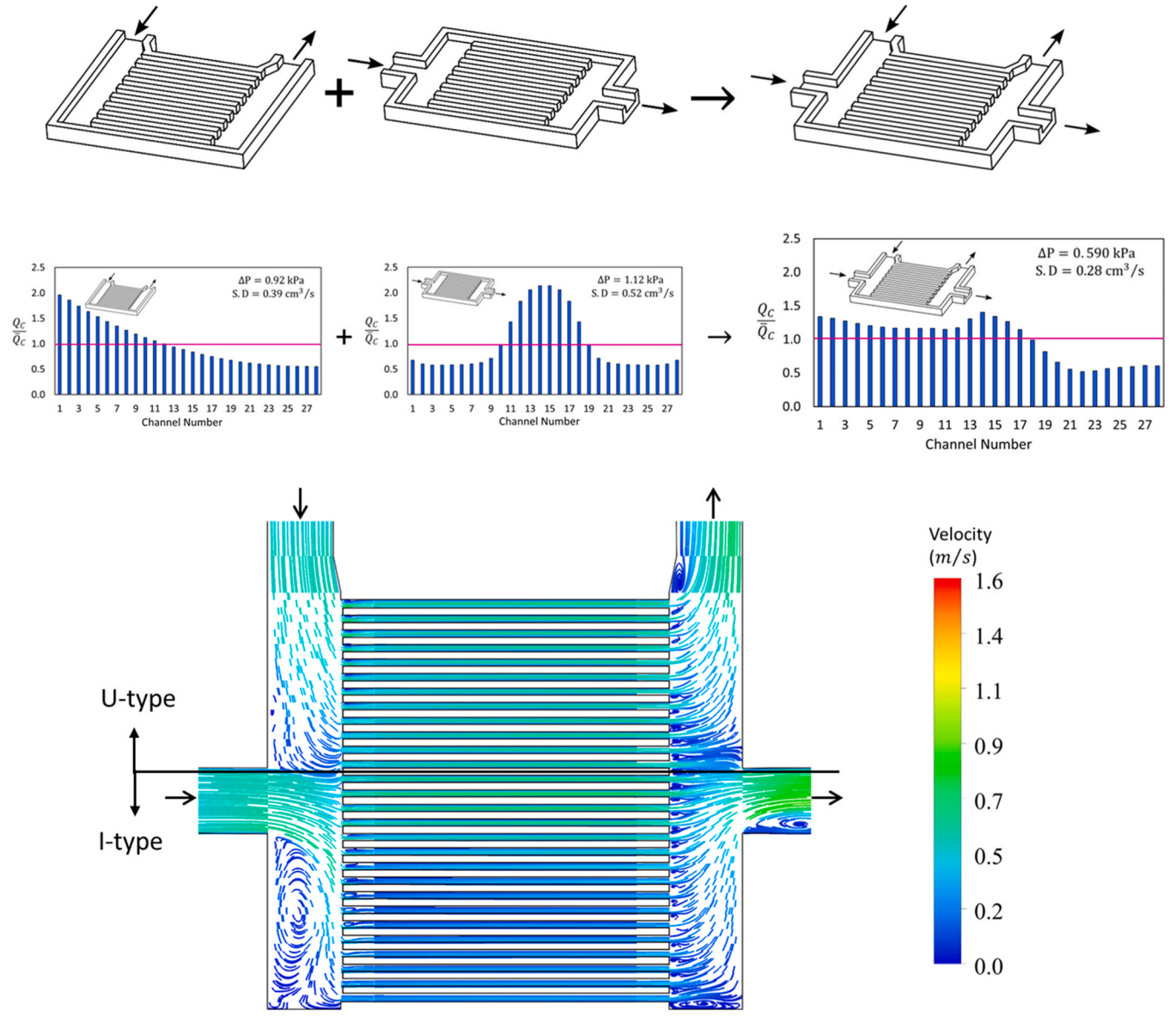

Fig. 24. Combination of U-type and I-type manifolds, flow distribution and pattern.

shaped distributor increases the flow rate of channels with less than average flow rate (8, 9, 20, and 21) and reducing the flow rate of channels with more than average flow rate (11–13 and 16–18), it does not improve flow uniformity significantly because of dramatic flow increase in channels next to jets. As it is expected, adding the vanes results in a higher pressure drop (65 %) because of the more friction and minor losses they cause.

Fig. 17(d) shows the flow distribution and pattern for a diffuser-nozzle shaped manifold with four guide vanes. Comparing the results of Fig. 17(d) with the results of two vanes manifold shown in Fig. 17(c), a substantial improvement is observed in flow uniformity (36 % reduction in flow standard deviation) without a significant pressure drop penalty (less than 2.5 % increase). Dividing the distributor to five sub-diffusers, provides more distributed jets with less momentum (Fig. 17(d) flow pattern) that brings the system in more flow uniformity. These jets, formed in the design with four vanes, from one side, direct the flow to the sides efficiently and from the other side increase the flow rate of the channels next to them more mildly than the jets formed in the two-vane system.

5.3. Combined parallel manifolds

The idea of combining N-type and U-type manifolds to approach a uniform flow distribution is developed as they have complementary flow distributions (Fig. 14). As can be seen in Fig. 14 in N-type manifold channel flow rate increases monotonically from the inlet to the end of distributor. The reverse trend occurs in the U-type manifold as the channel flow rate monotonically decreases by getting away from inlet duct. It is expected to approach a relatively uniform flow distribution by combining N-type and U-type manifolds sharing a same single inlet duct. Fig. 18 demonstrates the idea of combining N-type and U-type manifolds with a same inlet duct. As Fig. 18 shows the combined design has one inlet duct and both two outlet ducts of N-type and U-type manifolds. Both pressure drop and flow non-uniformity (flow standard deviation) significantly decrease in combined design compared to N-type and U-type manifolds. A reduction of 66 % and 60 % in pressure drop is obtained compared to N-type and U-type manifolds, respectively. Flow distribution standard deviation decreases in combined design by 71 % relative to N-type manifold and 56 % relative to U-type manifold. As the flow pattern in Fig. 18 illustrates the combined design can be divided to

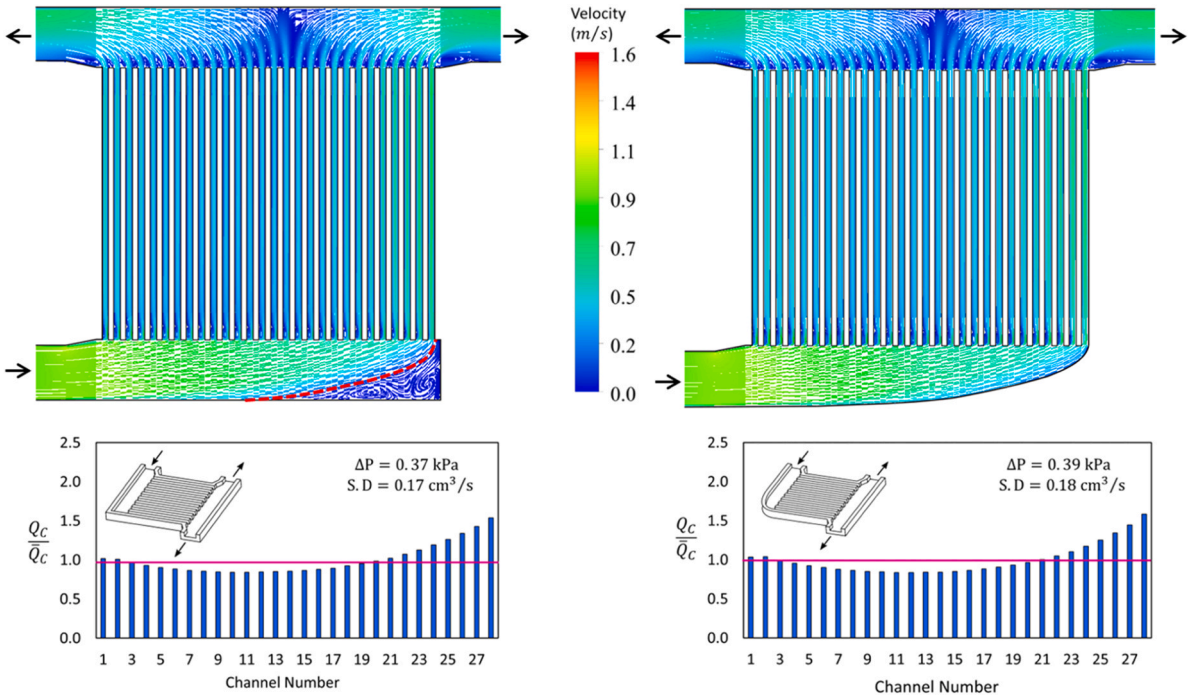

Fig. 25. Comparison of U+N type manifold and its streamlined version in flow distribution and pattern.

a U-type and an N-type manifold. Channels from number 1 to number 15 are involved in the U-type manifold and channels from number 17–28 share an N-type manifold. Both sets of channels are placed from the high flow rate regions of their own originals (channels close to inlet duct in U-type manifold and far from inlet duct in N-type manifold). In other words, two sets of channels reach a balance in receiving flow rate as those in the U-type manifold take the advantage of being close to inlet and outlet (short flow path) and those in the N-type manifold benefit from higher channel pressure gradient due to the Bernoulli's effect. It is worth to mention that a relatively uniform flow distribution is expected to be formed if both sets of channels in a combined design are taken from low-flow rate or high-flow rate regions in their original designs. In the combined design of Fig. 18 channels number 16 is the intersection of two sets of channels and the whole system is the union of the two sets. N-type and U-type manifolds are combined with a same outlet duct in Fig. 19. In this design, mainstream is divided to two equal flows each enters the system through separate inlet ducts opposite each other. The collector gathers the flow of all the channels and conducts it out through a single outlet duct. To have a consistent channel numbering in the combined and constituent designs, channel number increases by getting far from the outlets (Fig. 19). Flow standard deviation is obtained between those of the N-type and the U-type, close to their mean (0.49 cm^3/s), as the trend of flow distributions is the same (descending). Results show that no gain in pressure drop is obtained by combining N-type and U-type manifolds based on the common outlet duct. Here, again, the system is divided to two sets of channels having U-type (channels number 1–8) and N-type (channels number 8–28) manifolds.

As opposed to the previous case, in this design the channel sets are not positioned in the same flow rate (low or high flow rate) regions. Although channels of U-type set take the position of high flow rate, the channels of N-type set are from low flow rate position of N-type manifold (close to inlet). As a result, the combined system does not approach a uniform flow distribution. The combined design's flow standard deviation is less than that of the N-type manifold because the first eight channels are involved in the U-type manifold that provides less flow rate for them in comparison to the N-type manifold.

When working with manifolds with two inlets, adjacent eddies are formed to determine and separate the sets of channels. Fig. 19 shows two adjacent eddies formed in the inlet and divide the system to an N-type and U-type sets of channels.

The idea of combining complementary flow rate distributions to approach uniform distributions is applied to the Z-type and I-type manifolds in Fig. 20. As it can be seen, flow uniformity improves significantly by combining Z-type and I-type manifolds. Flow distribution standard deviation decreases by 75 % in the combined design relative to its constituents. The combined design presents a pressure drop 25 % and 65 % less than I-type and Z-type, respectively. As the flow pattern in Fig. 20 shows the whole systems is mainly divided to two Z-type manifolds beside each other. Indeed, except channels number 14 and 15 that receive flow from the middle inlet and discharge it to the middle outlet the rest of the channels are divided to two Z-type manifold sets. Here, again two adjacent eddies between the two inlets are formed and specify the two main Z-type sets.

Fig. 21 shows the combination of two reflective Z-type manifolds. Flow pattern and distribution of the combined design show that it could be considered as two I-type set halves of channels. Two adjacent symmetric eddies in the inlet divide the channels to two set with I-type manifolds. System pressure drop and flow distribution standard deviation are reduced by 74 % and 44 % from Z-type to combined design.

The combination of Z-type and N-type manifolds is illustrated in Fig. 22. The result shows that the pressure drop deceases by 74 % and 48 % comparing to Z-type and N-type manifolds, respectively. Reductions of 42 % and 49 % occurred in flow distribution standard deviation which shows more flow uniformity in the combined design in comparison to its constituents. Here, again eddies are formed and divide the channels to different sets. All channels that receive flow from inlet duct 1 discharge it to outlet duct 1 which is close to them. The same occurs for inlet duct 2 and outlet duct 2. The only exception is channels number 13 that receives flow from inlet duct 2 and discharge it to outlet 1 which follows the N-type manifold path.

Fig. 23 shows how the combination of two reflective U-type manifolds with complementary flow distribution reaches a design with considerably more uniform flow distribution (74 % reduction in S.D) and lower pressure drop (51 % reduction).

Fig. 24 illustrates the combination of U-type and I-type manifold which increases flow distribution uniformity and decreases system

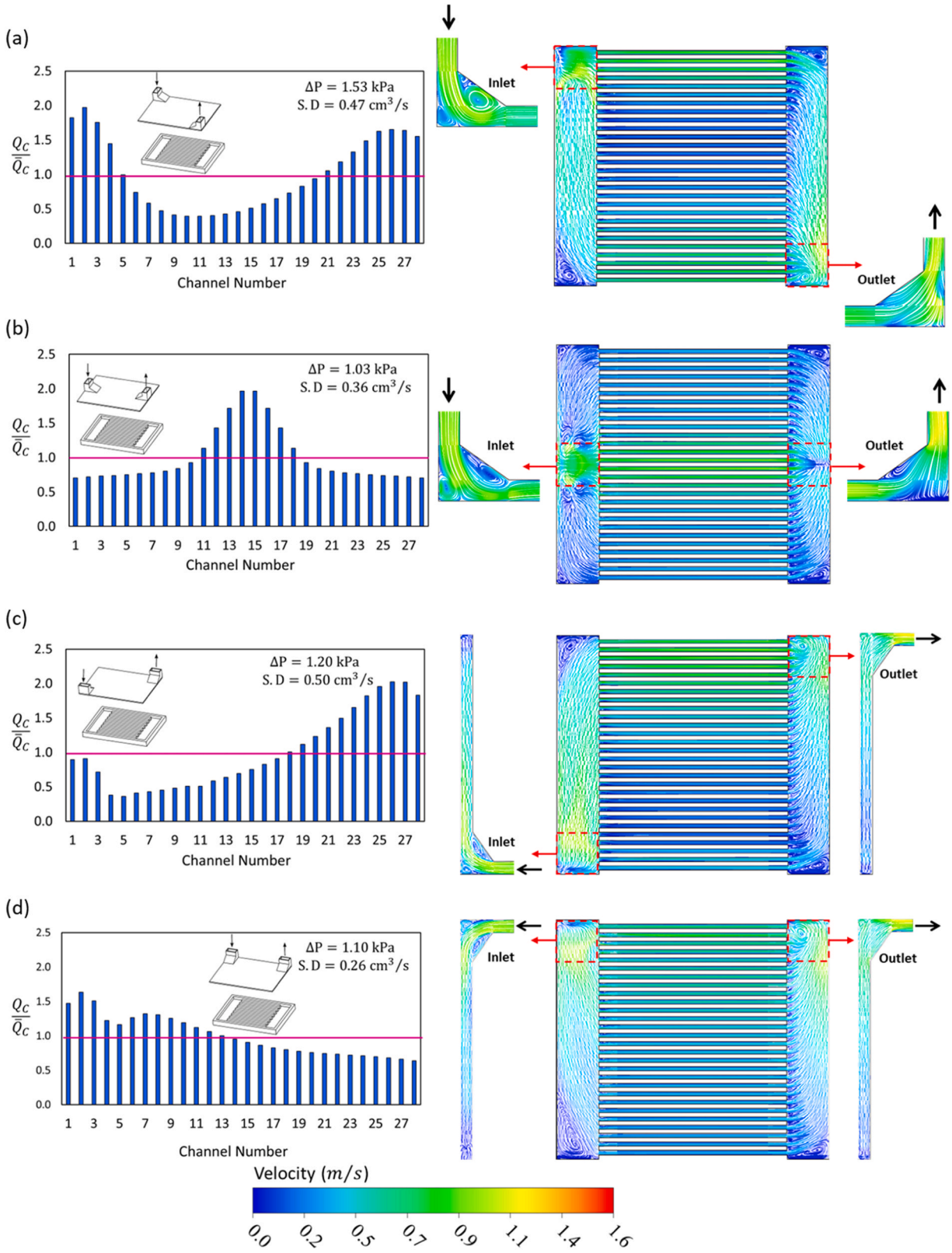

Fig. 26. Flow distribution and pattern for four basic vertical manifolds (a) VZ (b) VI (c) VN and (d) VU.

pressure drop. Because the flow distributions of these two manifold types are not complementary, the flow distribution non-uniformity and pressure drop do not meet its minimum values like in the combination of N- and U-, Z- and I-, and two reflective U-types.

5.4. Role of Eddies

When designing fluid dynamics devices and mechanisms, it is favored to diminish flow separation and eddy formation as much as

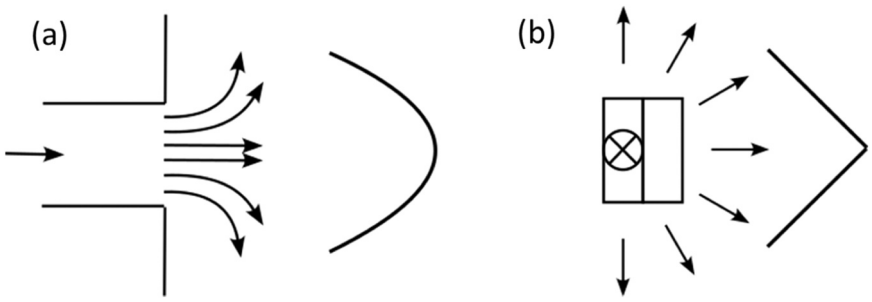

Fig. 27. (a) Flow distribution in middle channels of PI-type manifold and (b) VI-type manifold.

possible since they cause energy loss and degrade system performance. A typical example is subsonic diverging diffusers where adverse pressure gradient makes the boundary layer susceptible to separation. In general, reducing diffuser area ratio (A_{out}/A_{in}) and divergence angle fortify boundary layer against separation, by moderating adverse pressure gradient. Sudden expansion occurs in Z- and I-type manifolds generates large eddies (Fig. 14(a) and (b)) which result in flow energy loss. By decreasing the divergence angle, we expect to reach a higher-performance design. Applying this enhancement to I-type design (Fig. 17(a)) results in the diffuser-shaped design shown in Fig. 17(b). As can be seen in Figs. 17(a) and 17(b), from conventional I-type to diffuser-shaped design, although eddies shrink, no significant improvement (10 % reduction in pressure drop) is observed in system performance. To investigate the effect of eddies in inlet (dividing) manifolds, we chose the single inlet parallel U+N-type design (Fig. 18) to remove inlet manifold's eddies by streamlining it (Fig. 25). Although we expected an improvement in the system performance, like diffuser-shaped manifolds, no significant improvement was observed. Fig. 25 compares the flow distribution and pattern of the original and streamlined designs.

This lack of improvement in performance by shrinking eddies, stems from the main difference between diverging diffusers and manifolds which is flow branching. To diminish eddies (in both I- and N+U-type manifolds) we need to put walls close to channels along the flow. By getting close to the entrance of channels (branching regions), wall friction decreases the static pressure along the manifold which adversely affects velocity distribution and pressure drop. In our cases, the effect of the eddy shrinking and the effect of the interaction between flow branching and friction, offered by the walls, cancel each other out and result in same performance.

5.5. Basic vertical designs

Fig. 26 shows the results of flow distribution and pattern for four basic vertical inlet-outlet manifolds. As can be seen in Fig. 26(a) the vertical Z-type (VZ-type) manifold represents a flow distribution similar to that of the conventional parallel Z-type (PZ-type) shown in Fig. 14(a). Like PZ-type manifold, in VZ-type manifold, channels close to the inlet and outlet ducts receive more flow as they benefit from momentum effects of the inlet and outlet, respectively. An improvement of 10 % in flow uniformity (flow standard deviation) is observed as the momentum effects of the vertical inlet and outlet on their close channels are weaker than those of parallel inlet and outlets. This is due to the eddy formed in the inlet duct (Fig. 26(a)) and changes of 90° in flow direction in both inlet and outlet. A significant reduction of 36 % is observed in pressure drop from parallel to vertical Z-type manifold. PZ-type manifold offers higher pressure drop because of the sudden reduction in flow area occurs in the outlet duct as well as large eddies formed in the distributor.

Comparing the flow distribution of the parallel and vertical I-type manifolds (Figs. 14(b) and 26(b)), we realize that their trend is similar. Like in PI-type, in VI-type manifold, the channels in the middle receive more flow rate as they are closer to inlet and outlet ducts and provide short flow paths with low flow resistance. A significant improvement in flow uniformity of 31 % is obtain by switching from PI-type to VI-type with a slight reduction in pressure drop of 8 %. As Fig. 26(b) shows in VI-type manifold, the vertical inlet duct prevents eddies to be formed in the distributor (unlike in PI-type) and the whole volume of the distributor is used for fluid flow which results in more flow uniformity through channels. The flow distribution in the PI-type has a bell shape while in the VI-type manifold flow distribution has a triangular (linear ascending-descending) trend. This could be explained as in the PI-type manifold the channels in the middle (four channels for the current system) are in front of the inlet duct and receive the flow rate with small differences. Flow rate decreases dramatically in channels beside as to enter those channels fluid must deviate to the sides and pass the narrow passages between the large eddies and fins. In the VI-type manifold, flow distribution first decreases linearly by getting away from the middle and then approaches a plateau. By conducting the flow in different directions in the distributor evenly, the VI-type manifold provide a linear trend for channels in the middle and uniform distribution for channels on the sides. The schematic of Fig. 27 illustrates the bell-shaped and triangular trend in PI-type and VI-type manifolds.

Flow distribution trends of PN-type and VN-type manifolds are very similar (Figs. 14(c) and 26(c)). A reduction of 18 % occurs in flow distribution standard deviation from PN-type to VN-type manifold. Lower flow velocity at the beginning of the first three channels in the VN-type distributor than that in the PN-type results in higher channel inlet pressure and higher flow rate in these channels. The last three channels of the VN-type manifold receive lower flow rate than the corresponding channels in the PN-type manifold as the flow velocity is lower at the end of these channels in the collector of VN-type due to the minor loss of flow direction change to the top and larger outlet area. These reduction in the velocity at the end of the of last channels leads to their higher outlet pressure and lower flow rate. Pressure drop does not change significantly from PN-type to VN-type. Although VN-type provide slightly more uniform flow distribution (which reduce total pressure drop) the minor losses in inlet and outlet ducts (due to flow direction change and area) cancel the effect of flow more uniformity out and both designs provide almost equal pressure drops.

Comparing Figs. 14(d) and 26(d), one finds a reduction of 33 % in flow standard deviation and a growth of 20 % in pressure drop from PU-type to VU-type manifold. By shrinking eddies in the distributor and providing more uniform flow in both distributor and collector, VU-type manifold offers more uniform flow distribution than PU-type. VU-type manifold offers higher pressure drop than PU-type due to its minor losses.

5.6. Combined vertical manifolds

Fig. 28 shows the combination of VU-type and VN-type manifolds to approach more uniform flow distribution and lower pressure drop. Pressure drop decreases by 63 % and 60 % relative to VN-type and VU-type, respectively. Here, like the combination of parallel U-type and N-type manifolds, the combined design can be divided to a U-type and an

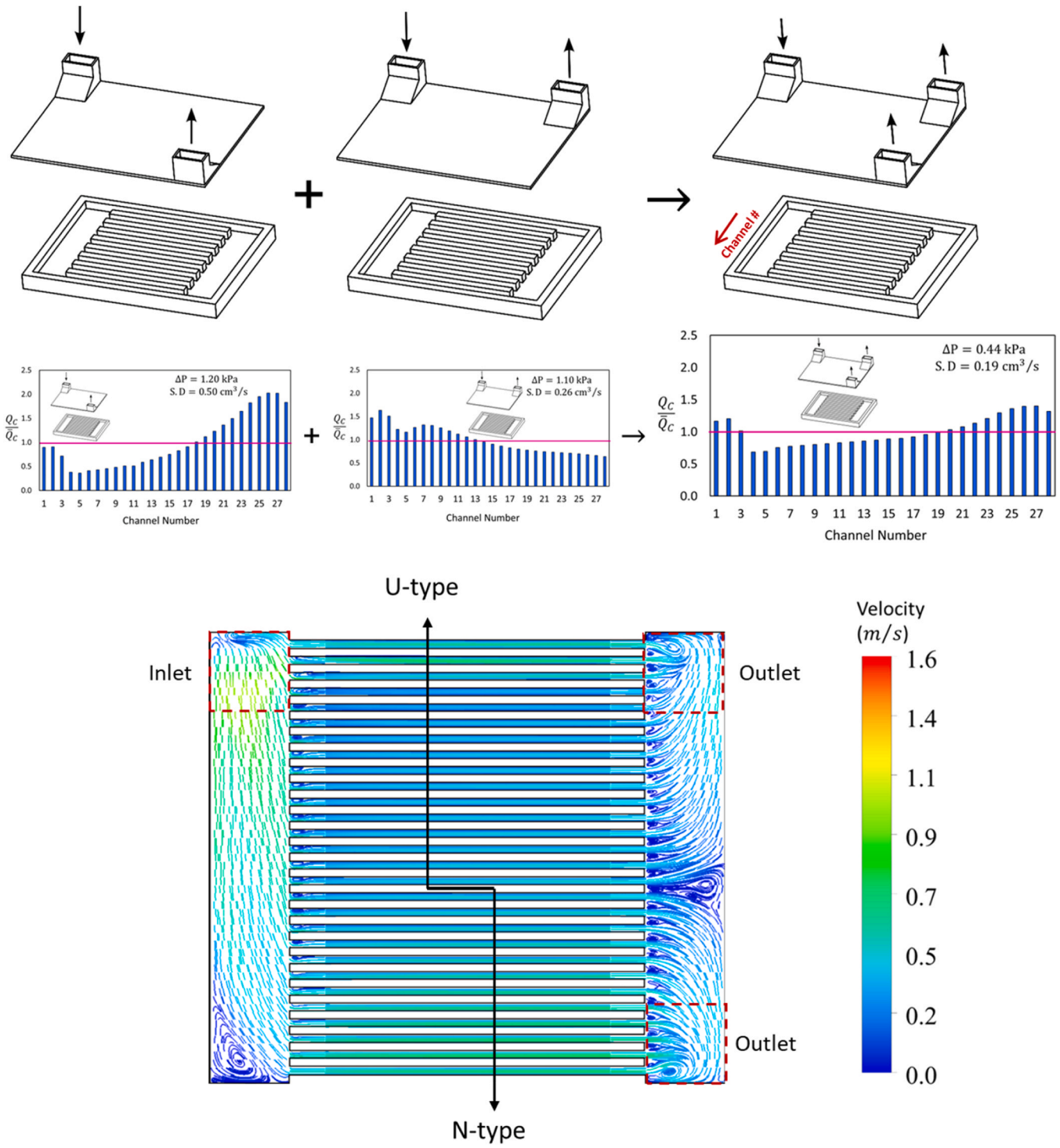

Fig. 28. Combination of VN-type and VU-type manifolds, flow distribution and pattern.

N-type manifolds. Channels from number 1 to number 16 are involved in a VU-type manifold and channels from number 17–28 share an VN-type manifold. By combining the two designs, reductions of 62 % and 27 % are obtained in the flow distribution standard deviation than VN-type and VU-type manifolds, respectively. More improvement is obtained in the parallel manifolds (Fig. 15) as the initial flow distributions are more complimentary in parallel designs than the vertical designs.

As like parallel Z- and I-type manifolds, vertical Z- and I-type manifolds possess complimentary flow distributions, their combination is modeled. Fig. 29 shows the obtained flow distribution and pattern of the combined design. As the flow pattern shows, channels are divided to two Z-type manifolds (1–12 and 19–28) and one I-type manifold (13–18). Significant reductions in pressure drop (63 % and 45 % relative to VZ-type and VI-type, respectively) and flow distribution standard deviation (70 % relative to VZ-type and 63 % relative to VI-type) are obtained as the initial designs flow distributions are complementary. Vertical ZI-type manifold shows lower pressure drop (by 33 %) than parallel ZI-type as the big eddies in the distributor are removed by vertical inlet duct.

The combination of two vertical Z-type manifolds is illustrated in Fig. 30. Significant reduction in pressure drop (67 %) and flow

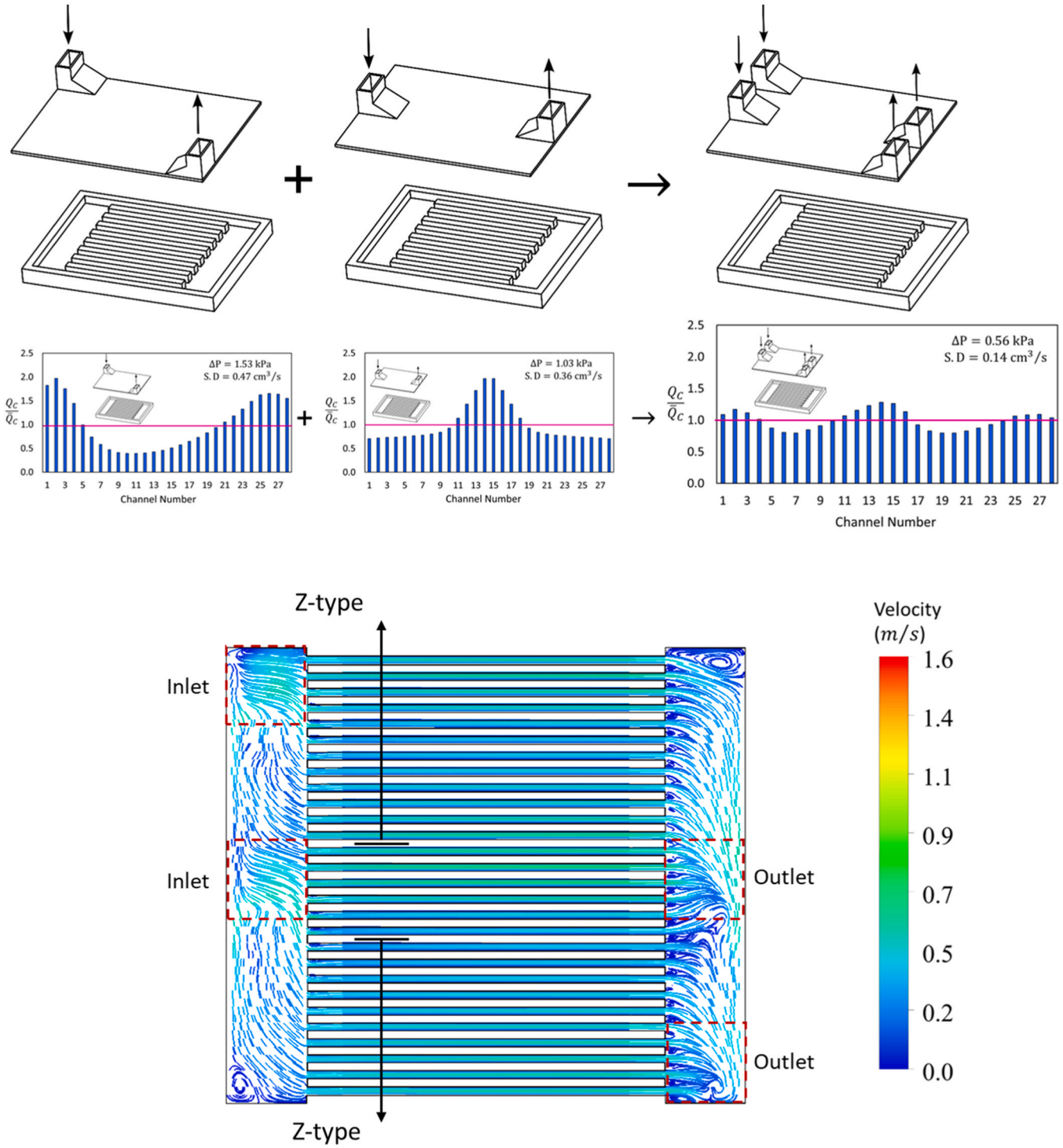

Fig. 29. Combination of VZ-type and VI-type manifolds, flow distribution and pattern.

distribution standard deviation (60 %) is obtained by combining two vertical Z-type manifolds. In comparison to the combination of two parallel Z-type manifolds, the combination of two vertical Z-type manifolds provides lower pressure drop (by 20 %) and flow standard deviation (by 34 %) as in vertical design, vertical inlet ducts eliminate big symmetric eddies.

The combination of vertical Z- and N-type manifolds are shown is Fig. 31. As it can be seen, the flow pattern is very similar to combination of vertical Z-type manifolds. Although the pressure drop of the designs of vertical Z+Z-type and vertical Z+N-type are quite similar, Z+N-type manifold provide a more uniform flow distribution (by 16 %) than vertical Z+Z-type manifold. Indeed, U- and N-type inlet ducts that supply the flow along the distribution outperform Z- and I-type inlet ducts that supply the flow toward the channels.

Fig. 32 illustrates the combination of vertical I -and Z-type manifolds. Although the flow distributions of these two designs are not complementary, reductions of 23 % and 44 % in flow distribution standard deviation are achieved by combining them compared to vertical U- and Z-type respectively. Pressure drop of the combined design is at least 50 % lower than the original designs. As the combined flow distribution

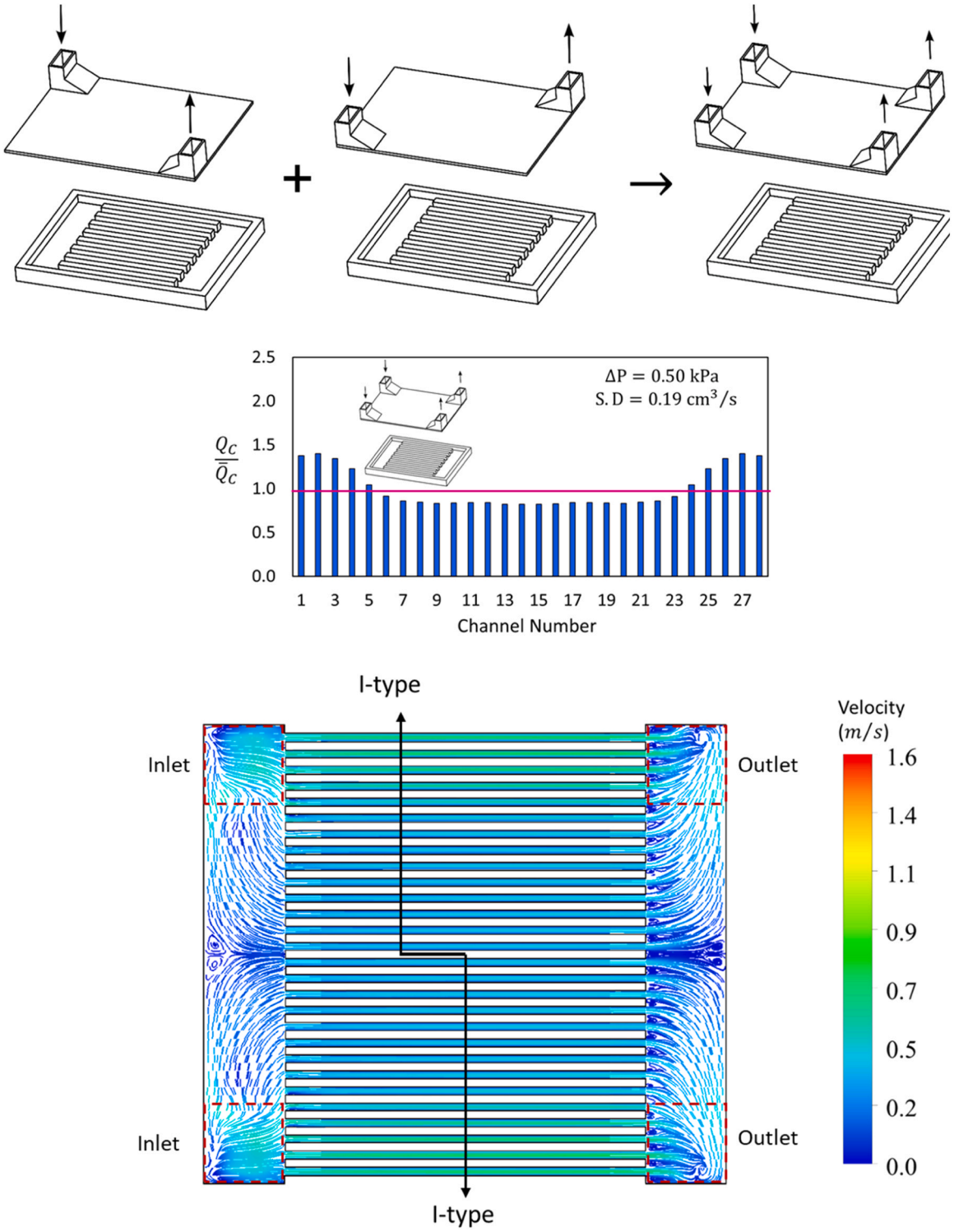

Fig. 30. Combination of two VZ-type manifolds, flow distribution and pattern.

shows the peak of the I-type design comes to the right side of peaks of the U-type design and divide the channels to two quasi-uniform flow groups 1–16 and 17–28.

Finally, the combination of two vertical U-type (or N-type) manifolds is demonstrated in Fig. 33. As can be seen, two U-type manifolds can be considered complementary provided that their inlet ducts and outlet ducts are placed opposite each other. Flow uniformity is remarkably improved by 92 % reduction in flow distribution standard deviation. Pressure drop also decreased substantially by 56 %. As the combined design's bar graph shows, flow distribution is very closed to ideally uniform flow with zero standard of deviation. The velocity profile is symmetric and shows that the whole system consists of two U-type systems mirrored.

5.7. Overview

In this study, pressure drop and flow distribution uniformity are considered as the response parameters for different manifold designs.

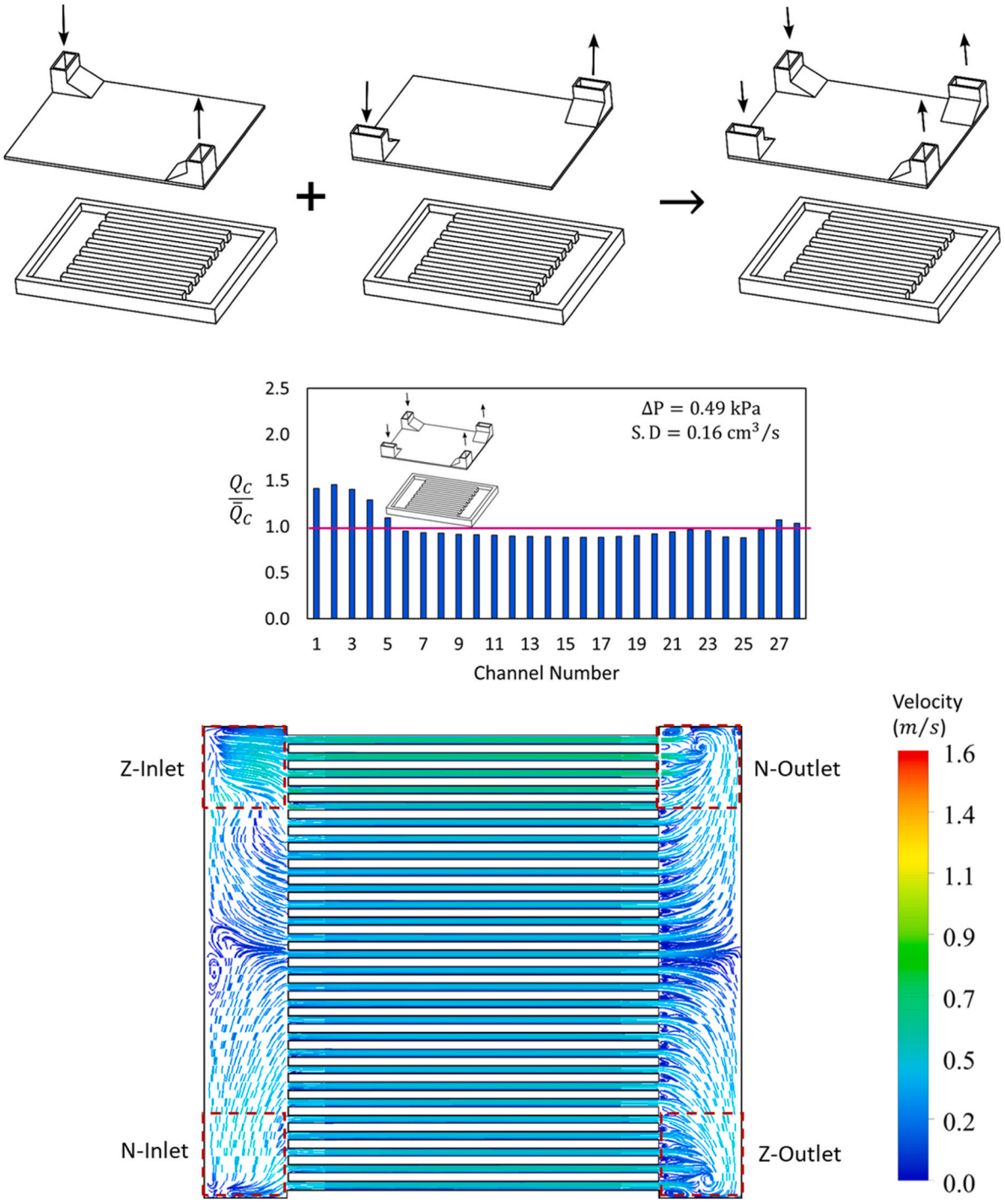

Fig. 31. Combination of VZ-type and VN-type manifolds, flow distribution and pattern.

Regardless of the system's application, we are interested in low pressure drop as it reduces both the probability of leaking and mechanical work needed to circulate the fluid. For flow uniformity, however, the situation could be different. In some applications, it is of practical interest to concentrate the flow over a special region. One example could be cooling electronic chips with non-uniform power map. Using I-type and Z-type manifolds is expected to enhance cooling a chip with a hot spot at the center and a chip with hot lines at the sides, respectively.

The results of pressure drop and flow uniformity for all designs studied are plotted in Fig. 34. As can be seen, the points do not follow a certain trend, we cannot imagine a general relation between system's pressure drop and flow uniformity. As the Fig. 34 shows, there is no point presenting high pressure drop and low flow standard deviation as well as no point with large flow distribution standard deviation and low pressure drop. The empty dashed trapezoid and triangle on Fig. 34 illustrate that system pressure drop depends on flow uniformity because a considerable part of the pressure drop occurs through the channels that decreases by uniforming flow distribution.

As expected, Fig. 34 shows that the points do not approach the ordinate as there is always a floor for the pressure drop across the system due to the friction in boundary layers. This pressure drop is the desired optimum value. But the points can approach the abscissa (as vertical U+U-type does) because there is no physical phenomenon prevents flow uniform distribution. It is observed from Fig. 34 that, parallel and

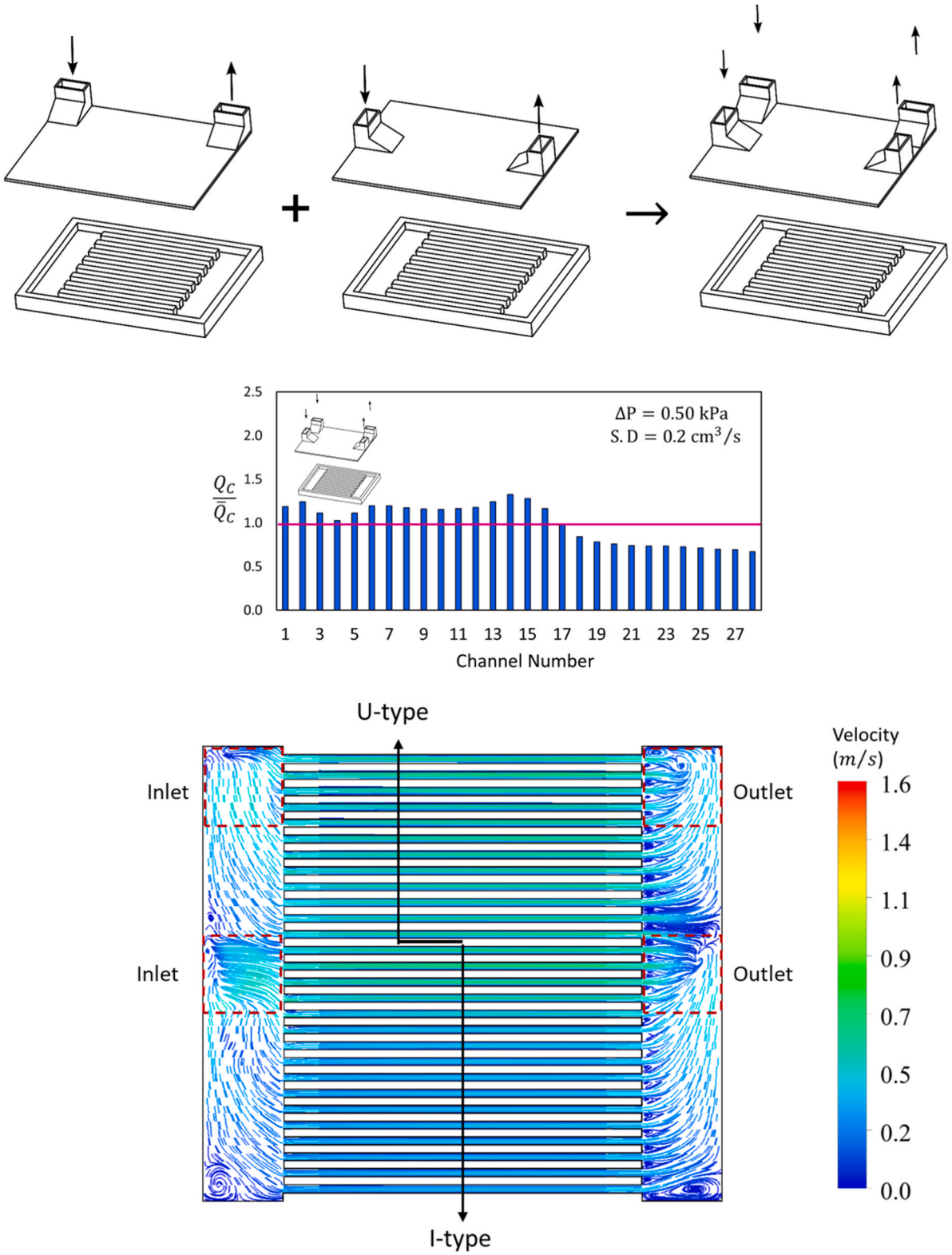

Fig. 32. Combination of VU-type and VI-type manifolds, flow distribution and pattern.

vertical designs with multiple outlets offer lower pressure drop. Double outlets split the exit velocity and increase outlet pressure. In other words, double outlet designs provide more flow exit area that results in lower pressure drop. The formation of big eddies in outlet ducts increases pressure drop as they act like solid barriers to block a part of flow exit area. Parallel Z-type manifold (the baseline) is a paradigm for this phenomenon. It should be noted that increasing number of inlet and outlet ducts does not necessarily improve the performance of the system. It is important to know how the inlet and outlet ducts position and direction affect pressure distribution at the beginning and end of the channels. Among the design points on diagram of Fig. 34, those with codes ID, ID2, and ID4 in red are I-type diffuser-shaped manifolds

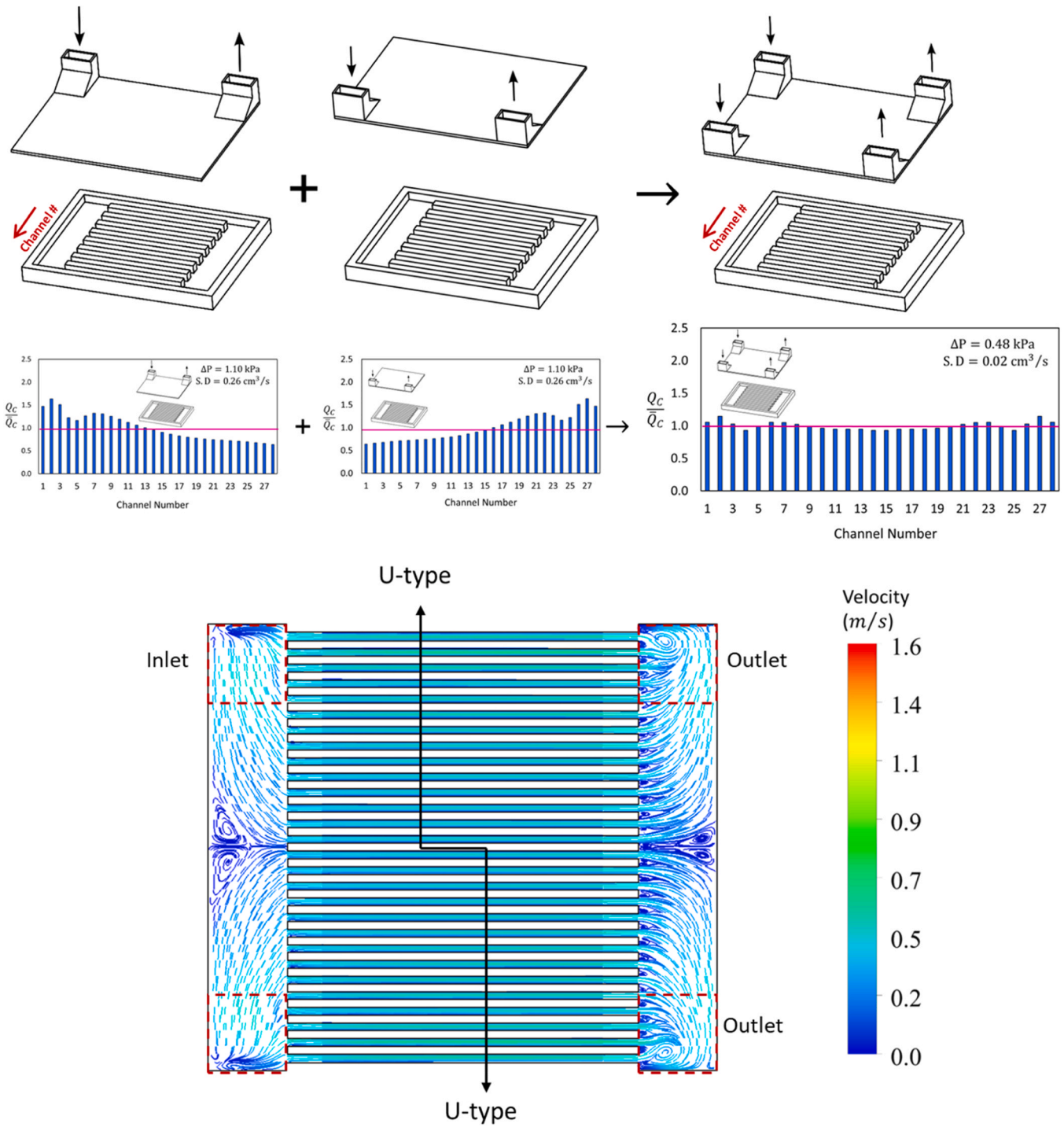

Fig. 33. Combination of two VU-type or two VN-type manifolds, flow distribution and pattern.

without, with two flow guides, and with four flow guides, respectively. Compering the design points of ID2 and ID4, we see that the design with four flow guide (ID4) provides more uniform flow distribution although its pressure drop is the same as the design with 2 flow guides (ID2). Indeed, the reduction in pressure drop because of more uniform flow distribution in ID4 is cancelled out by the adverse effect of more flow guides on pressure drop.

As Fig. 34 illustrates, parallel designs N+U and U+U and vertical design U+U have the minimum distance from the origin. This could be interpreted that among all the studied designs, these three designs have best performance. However, these outperforming designs can be sifted according to application, manufacturing, and cost-effectiveness perspective. As instance in more application including liquid-cooled heat sinks, server providers prefer parallel designed heat sinks due to space limitation and leak concerns. Indeed, transverse flow ducts need more room than in-plane ducts which results in thicker servers. In comparison to in-plane ducts, transverse ducts are more vulnerable to leaking as their coupling and fitting undergo more stress. Among the two remained parallel manifolds, N+U is preferred due to its simpler design. Indeed, single inlet makes the piping simpler and the whole system more robust against leak. Higher pressure upstream the channel network, brings the heat sinks inlets in higher risk of leak in comparison to outlets.

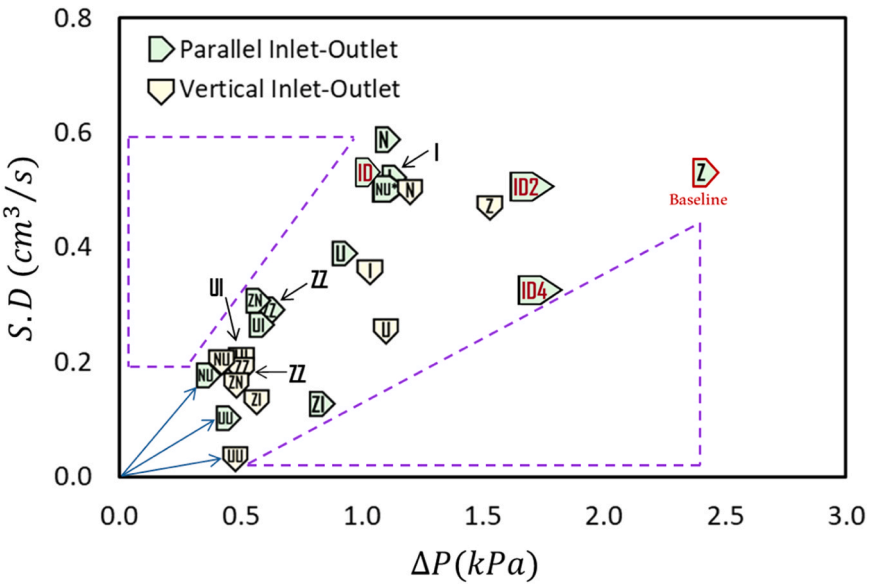

Fig. 34. The performance map of all designs solved.

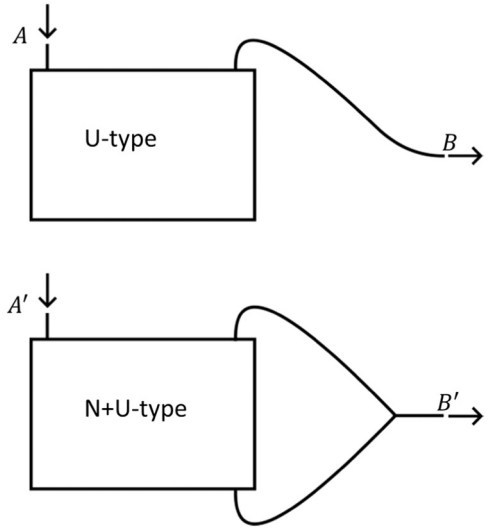

Fig. 35. Comparing piping of U-type and N+U-type manifolds.

Simpler designs are cost effective and easier to manufacture. This can be considered as an advantage for the design of N+U. Although by replacing parallel U-type manifold by parallel N+U-type manifold coolant must flow through two piece of hose and them merge through a Y-type junction (Fig. 35), still significantly lower pressure drop is offered by N+U-type manifold. Considering designs studied in this work and hoses with 10 cm length and 0.5 cm diameter downstream the device, N+U-type manifold provides a pressure drop 43 % less than U-type manifold ($\Delta p_{A'-B'} \leq 0.43\Delta p_{A-B}$). This pressure drop comparison is done with assumption of fully developed flow in hoses. As hoses entrance length increases by flow velocity, this reduction in pressure drop offered by N+U type manifold (43%) is the minimum achievable improvement.

6. Conclusion

In this study, a few ideas are generated for parallel channel systems' manifolds with the aim of minimizing flow non-uniformity and pressure drop. Three-dimensional computational models are developed and validated for pressure drop and flow distribution. The following conclusions are drawn from the present study:

(1) The idea of combining basic designs with complementary flow distribution trends presents designs with remarkably enhanced performance.
(2) Designs with vertical inlet/outlet ducts offer higher performance as they use more volume of distributor and collector. These designs, however, are vulnerable to leak, difficult to install, and occupy more space in vertical direction.
(3) Unlike in diffusers, in parallel channel systems' manifolds shrinking the eddies does not provide much improvement because of the interaction between branching of fluid and friction caused by walls. Both diffuser-shaped and streamlined manifolds do not show improvement than their originals. However, guide vanes can upgrade system performance.
(4) No explicit relation is observed between pressure drop and flow uniformity (Fig. 34) although pressure drop depends on flow distribution and is decreased by increasing flow uniformity. Indeed, both channel network and manifolds can dominantly contribute to total pressure drop depending on the design. Therefore, it is crucial to design manifolds with minimum contribution in system pressure drop.

CRediT authorship contribution statement

Ghazal Mohsenian: Visualization, Validation, Software, Resources, Methodology, Investigation, Formal analysis, Data curation. **Yaser Hadad:** Writing – review & editing, Writing – original draft, Visualization, Validation, Supervision, Methodology, Investigation, Formal analysis, Data curation, Conceptualization. **Bahgat Sammakia:** Supervision, Software, Resources, Investigation, Funding acquisition, Conceptualization. **Paul Chiarot:** Supervision, Resources, Project administration, Methodology, Investigation.

Declaration of Competing Interest

The authors declare that they have no known competing financial interests or personal relationships that could have appeared to influence the work reported in this paper.

Data Availability

Data will be made available on request.

Acknowledgements

This work was supported by NSF IUCRC Award IIP-1738793. The authors would like to acknowledge Profs. K. Ghose from Binghamton University, A. Ortega from Villavova University, D. Agonafer from University of Texas at Arlington, and Y. Joshi from Georgia Institute of Technology for their contribution in wining the award and support through the course of this study.

References

[1] A. Acrivos, B.D. Babcock, R.L. Pigford, Flow distributions in manifolds, Chem. Eng. Sci. 10 (1959) 112–124, https://doi.org/10.1016/0009-2509(59)80030-0.
[2] R.A. Bajura, A model for flow distribution in manifolds, J. Eng. Power 93 (1971) 7–12, https://doi.org/10.1115/1.3445410.
[3] R.A. Bajura, E.H. Jones Jr., Flow distribution manifolds, J. Fluids Eng. 98 (1976) 654–665, https://doi.org/10.1115/1.3448441.
[4] J.S. McNown, Mechanics of manifold flow, Trans. Am. Soc. Civ. Eng. 119 (1954) 1103–1118, https://doi.org/10.1061/TACEAT.0007058.
[5] R.L. Pigford, M. Ashraf, Y.D. Miron, Flow distribution in piping manifolds, Ind. Eng. Chem. Fund. 22 (1983) 463–471, https://doi.org/10.1021/i100012a019.
[6] K. Gocmen, H.S. Soyhan, An intake manifold geometry for enhancement of pressure drop in a diesel engine, Fuel 261 (2020) 116193, https://doi.org/10.1016/j.fuel.2019.116193.
[7] H. Talati, K. Aliakbari, A. Ebrahimi-Moghadam, H. Khoshbakht Farokhad, A. Eskandary Nasrabad, Optimal design and analysis of a novel variable-length intake manifold on a four-cylinder gasoline engine, Appl. Therm. Eng. 200 (2022) 117631, https://doi.org/10.1016/j.applthermaleng.2021.117631.
[8] G.R. de Souza, C. de C. Pellegrini, S.L. Ferreira, F. Soto Pau, O. Armas, Study of intake manifolds of an internal combustion engine: a new geometry based on experimental results and numerical simulations, Therm. Sci. Eng. Prog. 9 (2019) 248–258, https://doi.org/10.1016/j.tsep.2018.12.003.
[9] S. Maharudrayya, S. Jayanti, A.P. Deshpande, Pressure drop and flow distribution in multiple parallel-channel configurations used in proton-exchange membrane fuel cell stacks, J. Power Sources 157 (2006) 358–367, https://doi.org/10.1016/j.jpowsour.2005.07.064.
[10] R.J. Kee, P. Korada, K. Walters, M. Pavol, A generalized model of the flow distribution in channel networks of planar fuel cells, J. Power Sources 109 (2002) 148–159, https://doi.org/10.1016/S0378-7753(02)00090-3.
[11] W. Zhang, P. Hu, X. Lai, L. Peng, Analysis and optimization of flow distribution in parallel-channel configurations for proton exchange membrane fuel cells, J. Power Sources 194 (2009) 931–940, https://doi.org/10.1016/j.jpowsour.2009.05.033.
[12] J. Dong, X. Xu, B. Xu, CFD analysis of a novel modular manifold with multi-stage channels for uniform air distribution in a fuel cell stack, Appl. Therm. Eng. 124 (2017) 286–293, https://doi.org/10.1016/j.applthermaleng.2017.06.030.
[13] C.-H. Chen, S.-P. Jung, S.-C. Yen, Flow distribution in the manifold of PEM fuel cell stack, J. Power Sources 173 (2007) 249–263, https://doi.org/10.1016/j.jpowsour.2007.05.007.
[14] J. Wang, H. Wang, Discrete approach for flow field designs of parallel channel configurations in fuel cells, Int. J. Hydrog. Energy 37 (2012) 10881–10897, https://doi.org/10.1016/j.ijhydene.2012.04.034.
[15] S. Maharudrayya, S. Jayanti, A.P. Deshpande, Flow distribution and pressure drop in parallel-channel configurations of planar fuel cells, J. Power Sources 144 (2005) 94–106, https://doi.org/10.1016/j.jpowsour.2004.12.018.
[16] J. Wang, Pressure drop and flow distribution in parallel-channel configurations of fuel cells: U-type arrangement, Int. J. Hydrog. Energy 33 (2008) 6339–6350, https://doi.org/10.1016/j.ijhydene.2008.08.020.
[17] J. Wang, Pressure drop and flow distribution in parallel-channel configurations of fuel cells: Z-type arrangement, Int. J. Hydrog. Energy 35 (2010) 5498–5509, https://doi.org/10.1016/j.ijhydene.2010.02.131.
[18] J. Wang, Theory of flow distribution in manifolds, Chem. Eng. J. 168 (2011) 1331–1345, https://doi.org/10.1016/j.cej.2011.02.050.
[19] J.M. Commenge, L. Falk, J.P. Corriou, M. Matlosz, Optimal design for flow uniformity in microchannel reactors, AIChE J. 48 (2002) 345–358, https://doi.org/10.1002/aic.690480218.
[20] K. Zygourakis, Transient operation of monolith catalytic converters: a two-dimensional reactor model and the effects of radially nonuniform flow distributions, Chem. Eng. Sci. 44 (1989) 2075–2086, https://doi.org/10.1016/0009-2509(89)85143-7.
[21] B. Thonon, P. Mercier, M. Feidt, Flow distribution in plate heat exchangers and consequences on thermal and hydraulic performances, in: W. Roetzel, P.J. Heggs, D. Butterworth (Eds.), Design and Operation of Heat Exchangers, Springer, Berlin, Heidelberg, 1992, pp. 245–254, https://doi.org/10.1007/978-3-642-84450-8_23.
[22] B.P. Rao, S.K. Das, An experimental study on the influence of flow maldistribution on the pressure drop across a plate heat exchanger, J. Fluids Eng. 126 (2004) 680–691, https://doi.org/10.1115/1.1779664.
[23] M.K. Bassiouny, H. Martin, Flow distribution and pressure drop in plate heat exchangers—I U-type arrangement, Chem. Eng. Sci. 39 (1984) 693–700, https://doi.org/10.1016/0009-2509(84)80176-1.
[24] L. Beckedorff, R.P.P. da Silva, G.S.M. Martins, K.V. de Paiva, J.L.G. Oliveira, A.A. M. Oliveira, Flow maldistribution and heat transfer characteristics in plate and shell heat exchangers, Int. J. Heat. Mass Transf. 195 (2022) 123182, https://doi.org/10.1016/j.ijheatmasstransfer.2022.123182.
[25] Y. Hao, Y. Wang, T. Hu, The flow distribution in the parallel tubes of the cavity receiver under variable heat flux, Appl. Therm. Eng. 108 (2016) 641–649, https://doi.org/10.1016/j.applthermaleng.2016.07.168.
[26] J. Liu, J. Pan, L. Tang, X. Su, Modeling and analysis of steam-water two-phase flow distribution and wall temperature distribution in parallel heated pipes with different manifold types, Appl. Therm. Eng. 210 (2022) 118387, https://doi.org/10.1016/j.applthermaleng.2022.118387.
[27] R. Uhlig, B. Gobereit, J. Rheinländer, Advancing tube receiver performance by using corrugated tubes, Energy Procedia 69 (2015) 563–572, https://doi.org/10.1016/j.egypro.2015.03.065.
[28] M. Saeed, M.-H. Kim, Header design approaches for mini-channel heatsinks using analytical and numerical methods, Appl. Therm. Eng. 110 (2017) 1500–1510, https://doi.org/10.1016/j.applthermaleng.2016.09.069.
[29] D. Bogojevic, K. Sefiane, A.J. Walton, J.R.E. Christy, G. Cummins, H. Lin, Investigation of flow distribution in microchannels heat sinks, Heat. Transf. Eng. 30 (2009) 1049–1057, https://doi.org/10.1080/01457630902921287.
[30] E.S. Cho, J.W. Choi, J.S. Yoon, M.S. Kim, Modeling and simulation on the mass flow distribution in microchannel heat sinks with non-uniform heat flux conditions, Int. J. Heat. Mass Transf. 53 (2010) 1341–1348, https://doi.org/10.1016/j.ijheatmasstransfer.2009.12.025.
[31] O. Tonomura, S. Tanaka, M. Noda, M. Kano, S. Hasebe, I. Hashimoto, CFD-based optimal design of manifold in plate-fin microdevices, Chem. Eng. J. 101 (2004) 397–402, https://doi.org/10.1016/j.cej.2003.10.022.
[32] D. Tondeur, Y. Fan, J.-M. Commenge, L. Luo, Uniform flows in rectangular lattice networks, Chem. Eng. Sci. 66 (2011) 5301–5312, https://doi.org/10.1016/j.ces.2011.07.027.
[33] M.-C. Lu, C.-C. Wang, Effect of the inlet location on the performance of parallel-channel cold-plate, IEEE Trans. Compon. Packag. Technol. 29 (2006) 30–38, https://doi.org/10.1109/TCAPT.2005.850539.
[34] G.D. Xia, J. Jiang, J. Wang, Y.L. Zhai, D.D. Ma, Effects of different geometric structures on fluid flow and heat transfer performance in microchannel heat sinks, Int. J. Heat. Mass Transf. 80 (2015) 439–447, https://doi.org/10.1016/j.ijheatmasstransfer.2014.08.095.
[35] J.-Y. Song, S. Hah, D. Kim, S.-M. Kim, Enhanced flow uniformity in parallel mini-channels with pin-finned inlet header, Appl. Therm. Eng. 152 (2019) 718–733, https://doi.org/10.1016/j.applthermaleng.2019.02.069.
[36] R. Manikanda Kumaran, G. Kumaraguruparan, T. Sornakumar, Experimental and numerical studies of header design and inlet/outlet configurations on flow mal-distribution in parallel micro-channels, Appl. Therm. Eng. 58 (2013) 205–216, https://doi.org/10.1016/j.applthermaleng.2013.04.026.
[37] C. Anbumeenakshi, M.R. Thansekhar, Experimental investigation of header shape and inlet configuration on flow maldistribution in microchannel, Exp. Therm. Fluid Sci. 75 (2016) 156–161, https://doi.org/10.1016/j.expthermflusci.2016.02.004.
[38] E.S. Cho, J.W. Choi, J.S. Yoon, M.S. Kim, Experimental study on microchannel heat sinks considering mass flow distribution with non-uniform heat flux conditions, Int. J. Heat. Mass Transf. 53 (2010) 2159–2168, https://doi.org/10.1016/j.ijheatmasstransfer.2009.12.026.
[39] J.C.K. Tong, E.M. Sparrow, J.P. Abraham, Geometric strategies for attainment of identical outflows through all of the exit ports of a distribution manifold in a manifold system, Appl. Therm. Eng. 29 (2009) 3552–3560, https://doi.org/10.1016/j.applthermaleng.2009.06.010.
[40] R. Chein, J. Chen, Numerical study of the inlet/outlet arrangement effect on microchannel heat sink performance, Int. J. Therm. Sci. 48 (2009) 1627–1638, https://doi.org/10.1016/j.ijthermalsci.2008.12.019.
[41] T.-H. Shih, W.W. Liou, A. Shabbir, Z. Yang, J. Zhu, A new k-ϵ eddy viscosity model for high reynolds number turbulent flows, Comput. Fluids 24 (1995) 227–238, https://doi.org/10.1016/0045-7930(94)00032-T.
[42] S.B. Pope, Higher Education from. Turbulent Flows, Cambridge University Press, 2000, https://doi.org/10.1017/CBO9780511840531.
[43] RobertL. Mott, Applied Fluid Mechanics, sixth, PERSOM Prentice Hall, New Jersey, 2006.
[44] Y.S. Muzychka, M.M. Yovanovich, Pressure drop in laminar developing flow in noncircular ducts: a scaling and modeling approach, J. Fluids Eng. 131 (2009), https://doi.org/10.1115/1.4000377.
[45] Z. Duan, M.M. Yovanovich, Y.S. Muzychka, Pressure drop for fully developed turbulent flow in circular and noncircular ducts, J. Fluids Eng. 134 (2012) 061201, https://doi.org/10.1115/1.4006861.
[46] FrankM. White. Fluid Mechanics, 7th ed., McGraw-Hill, New York, USA, 2011.
[47] RobertD. Blevins. Applied Fluid Dynamics Handbook, 1st ed., Krieger Pub Co, New York, USA, 1984.
[48] DonaldS. Miller. Internal Flow Systems, 2nd ed., BHRA, Cranfield, UK, 1990.